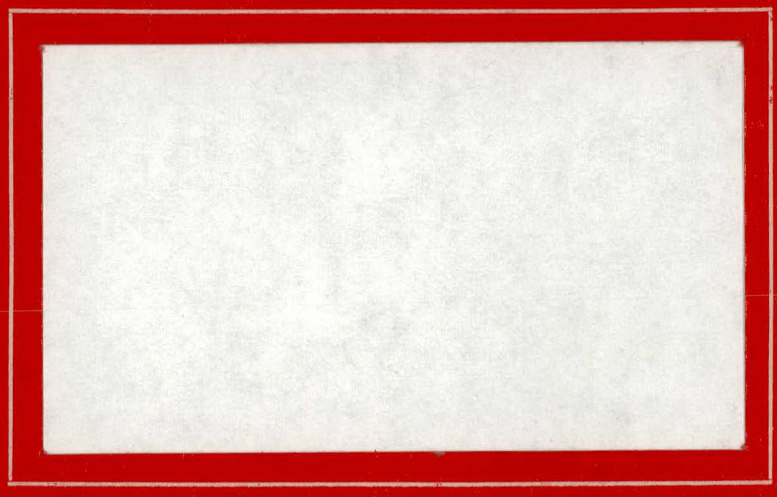

Rensselaer Polytechnic Institute

Troy, New York 12181

DISCLAIMER

COO-3058-21

LINEAR ACCELERATOR PROJECT

AEC Contract No. AT(11-1)-3058

PROGRESS REPORT

for

April 1, 1972 - June 30, 1972

Rensselaer Polytechnic Institute
Troy, New York 12181

E.R. Gaerttner

Erwin R. Gaerttner
Project Director

TABLE OF CONTENTS

NEUTRON CROSS SECTIONS

TOTAL NEUTRON CROSS SECTION ON HELIUM AND ^{6}LI

C. A. Goulding* and P. Stoler

The total cross-section measurement of neutrons on He has been completed. The data were taken in two separate blocks of running time. The first was of 72 hours duration; the second, of 40 hours. In both cases the electron beam burst width was 20 nsec with an energy of 70 Mev. As reported previously,[1] the energy resolution in the first run was reduced to 40 nsec per channel due to jitter in the ADC. However, in the second run, the data were taken with the EG&G TDC500 Time Digitizer. The Time Digitizer not only allows us to select channel widths as small as 1/8 nsec, but also eliminates the need for the ADC and the time jitter problems associated with it. In the latter experiment we chose the channel width to be 4 nsec. The Time Digitizer will be covered in more detail in a later report.

In order to improve the statistics on the data above 15 Mev, in the second run we ran with a thicker sample. To attain this, we first connected the sample holder to a bottle of 99.99% He at 400 Psi. The sample holder was then immersed in liquid helium and the bottle valve was opened. After a wait of a few minutes, the valves on the bottle and sample holder were closed and the sample holder removed from the liquid helium. With this cryopumping, we were able to get a pressure of 2943 Psi or a sample thickness of 0.489 atoms/barn as compared to 0.301 for the first run. Also, to improve the higher energy data, we took data with two detector modules and maximum beam current which resulted in the detection of about three neutrons per machine burst. This increased the data-taking at high energy (above 10 Mev), but also greatly increased the deadtime at low energies. Figure 1 shows the good agreement of the data from the first run with that of the second. The first run used the ADC, a smaller sample thickness, and

*Based in part on the Ph.D. Thesis of C. A. Goulding.

smaller deadtime corrections — whereas the second used the EG&G Time Digitizer, a thicker sample, and higher deadtime corrections. All data are averaged to 40 nsec.

Considering the marked differences in experimental conditions between the two runs, the agreement is quite good. This agreement is particularly significant in the region of the 1.1 MeV peak, where transmission is small. The ratio of true counts to background at the peak is 3.5 for the latter run and thus improper background subtraction would introduce a large error in the calculated cross section. Furthermore, the deadtime correction at this energy for the latter run is about 75 percent for the sample-out position. The good agreement between the two runs gives us confidence that the deadtime corrections are basically accurate, and the flat background assumption is justified above 1 Mev in the Mev experiments.

Until the present, there was a wide gap of 2 Mev at 8 Mev neutron energy in which there were no data available, and the scatter of points between 14 and 20 Mev was from about 0.3 to 1.5 barns. Figures 2, 3 and 4 show the present data in comparison with that of LASL.[4] It can be seen that the agreement is quite good over the entire energy range.

Figures 5, 6 and 7 show the ^{6}Li data reported previously.[2] This represents about ninety-six hours of running time at 60 Mev with a burst width of 20 nsec. Figure 5 shows a comparison of our data with that of Meadows and Whalen.[5] While the energy resolution of our data is lower, the statistical error is less and it can be seen that the agreement is within 1%. Figures 6 and 7 show a comparison of our data with that of Glasgow and Foster.[6] While the agreement is good at lower energy, the Glasgow and Foster data start to drop below the present set at 5 Mev and continues to be lower until 15 Mev where the disagreement is about 5%. Figure 8 shows a comparison of the ^{7}Li cross section[3] with that of ^{6}Li.

REFERENCES:

1. Linear Accelerator Project Progress Report - January - March 1972, COO-3058-14.

2. Ibid., p. 5.

3. Linear Accelerator Project Annual Technical Report, October 1, 1970 - September 30, 1971, COO-3058-1.

4. National Neutron Cross Section Center, Brookhaven National Laboratory, private communication.

5. J. W. Meadows and J. F. Whalen, data obtained from National Neutron Cross Section Center, Brookhaven National Laboratory.

6. D. G. Foster and D. W. Glasgow, Phys. Rev., 3, 576 (1971). Data obtained from National Neutron Cross Section Center, Brookhaven National Laboratory.

FIGURE CAPTIONS

Fig. 1 Helium Total Neutron Cross Section from 1.0 to 30 Mev. Solid line represents data from the first run; vertical bars, the data from the second run. The size of the bar reflects the size of the statistical error.

Fig. 2 Helium Total Neutron Cross Section from 0.7 to 2 Mev. Vertical bars are the statistical error with the solid line drawn to guide the eye. The +'s at 0.94, 1.50 and 1.98 Mev are the LASL[4] data.

Fig. 3 Helium Total Neutron Cross Section from 2.0 to 15.0 Mev. Vertical bars are the statistical error for the present data with the +'s representing the LASL data.

Fig. 4 Helium Total Neutron Cross Section from 15.0 to 30 mev. Vertical bars are the statistical error for the present data with the +'s representing the LASL data.

Fig. 5 ^{6}Li Total Neutron Cross Section from 0.7 to 2.0 Mev. Vertical bars are the statistical error in the present data with the solid line drawn to guide the eye. The +'s are the data of Meadows and Whalen.[5]

Fig. 6 ^{6}Li Total Neutron Cross Section from 2.0 to 10.0 Mev. Vertical bars are the statistical error in the present data. The +'s are the data of Glasgow and Foster.[6]

Fig. 7 ^{6}Li Total Neutron Cross Section from 10.0 to 30 Mev. Vertical bars are the statistical error in the present data with the solid line drawn to guide the eye. The +'s are the data of Glasgow and Foster.

Fig. 8 A Comparison of the Total Neutron Cross Section of ^{7}Li with that of ^{6}Li. The +'s represent the present ^{6}Li data. The solid line represents the ^{7}Li data which was reported in Ref. 3.

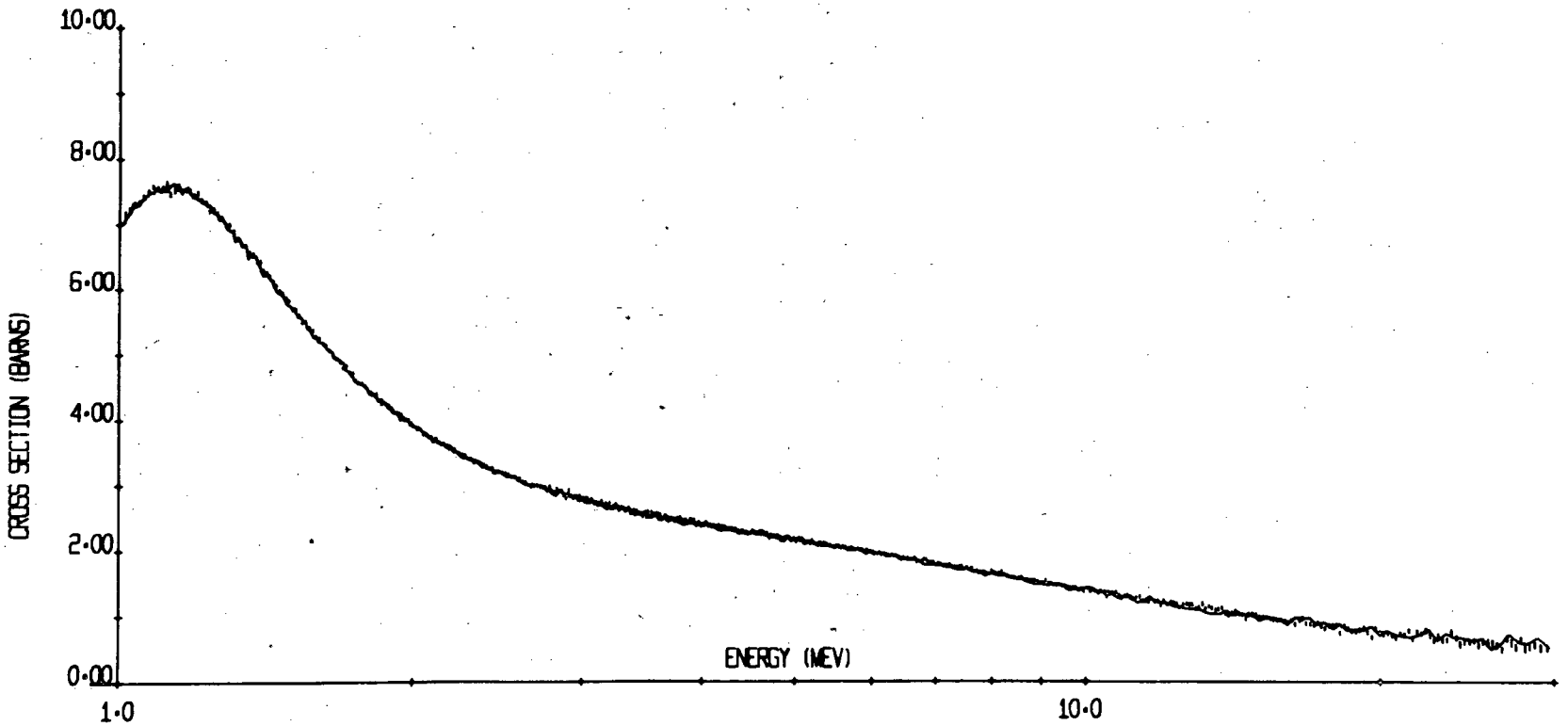
10·00
8·00
6·00
4·00
2·00
0·00
CROSS SECTION (BARNS)
ENERGY (MEV)
1·0
10·0

Figure 1

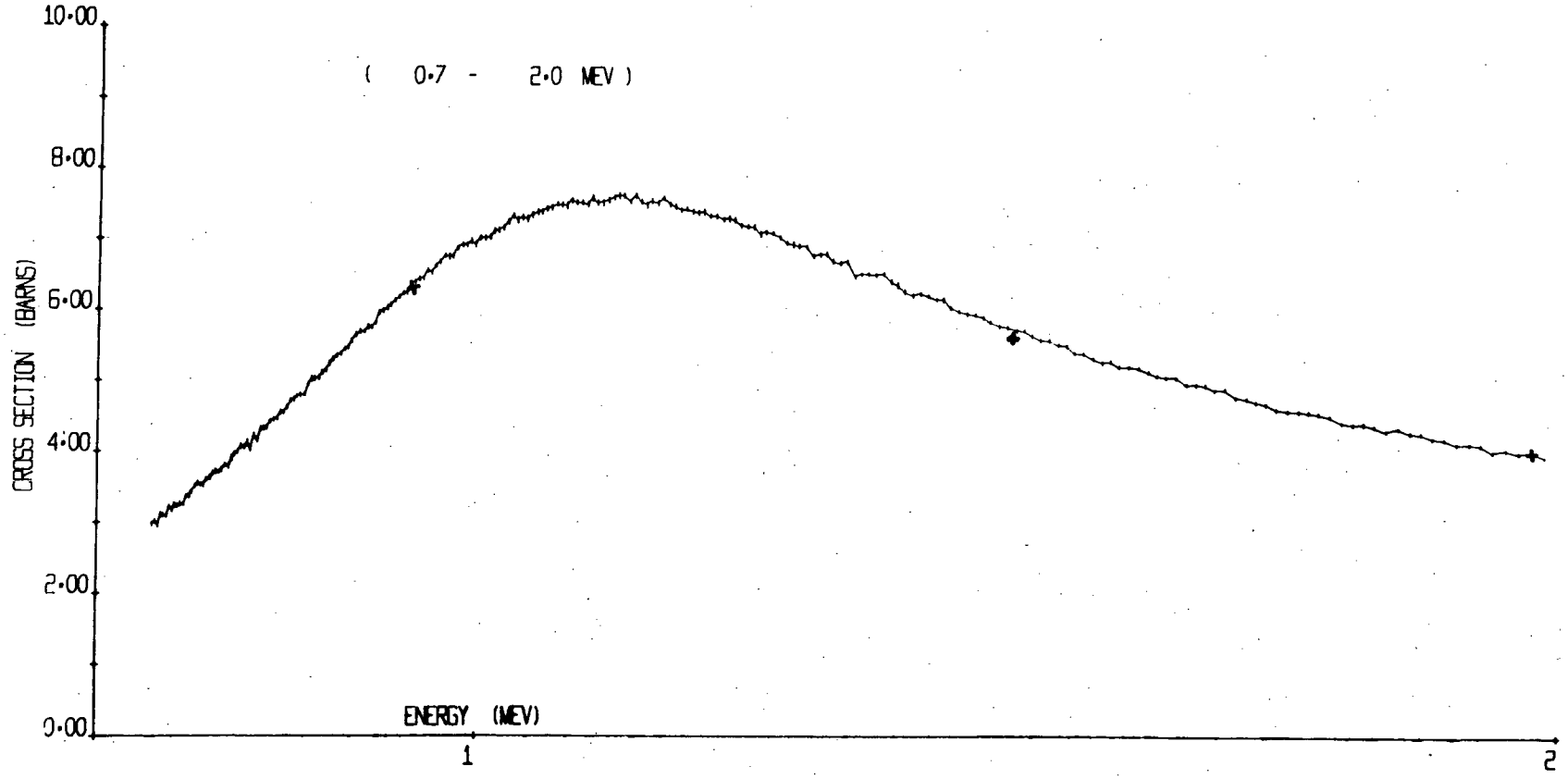
10·00
8·00
6·00
4·00
2·00
0·00
(0·7 - 2·0 MEV)
CROSS SECTION (BARNS)
ENERGY (MEV)
1
2

Figure 2

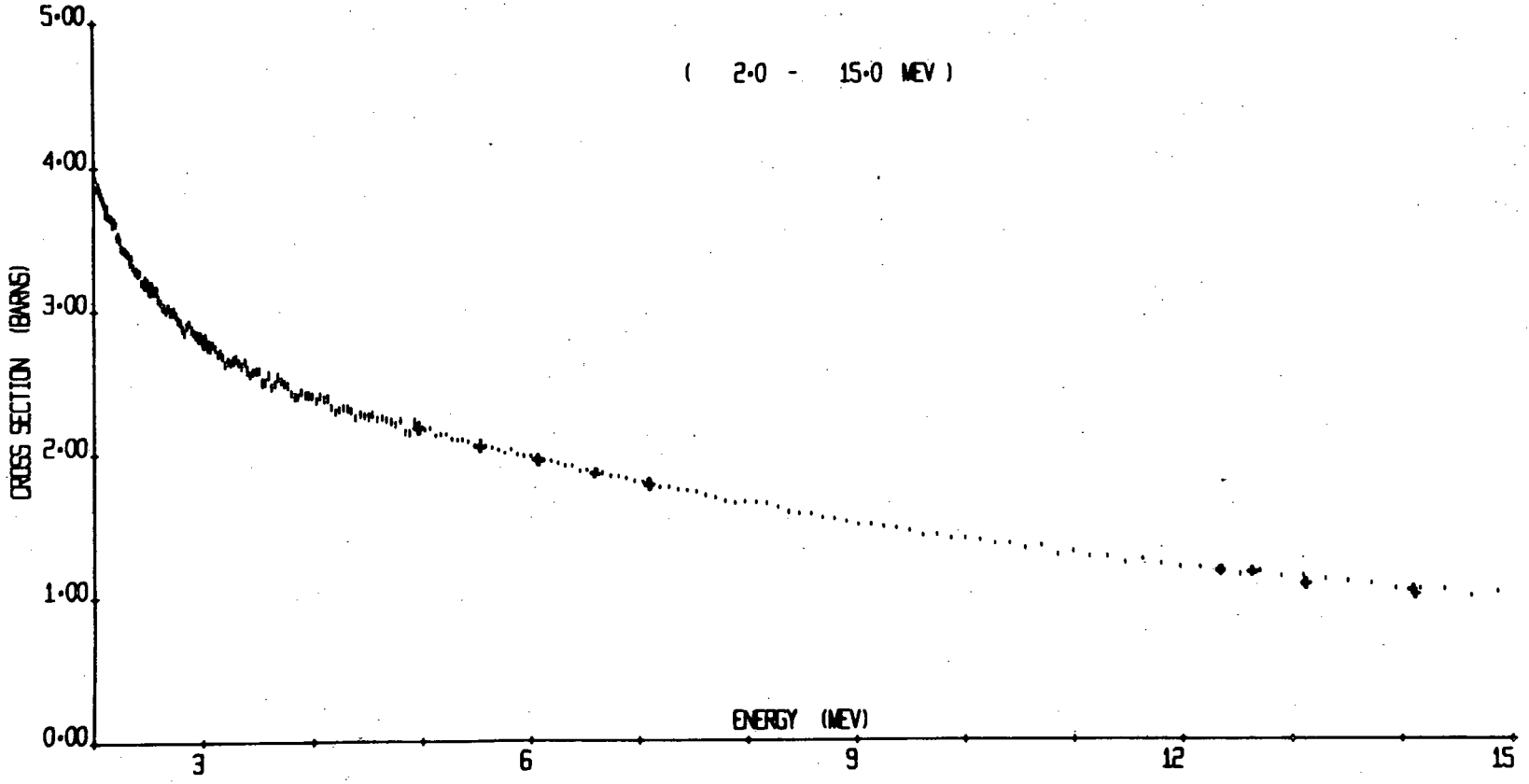
(2·0 - 15·0 MEV)
5·00
4·00
3·00
2·00
1·00
0·00
CROSS SECTION (BARNS)
3
6
9
12
15
ENERGY (MEV)

Figure 3

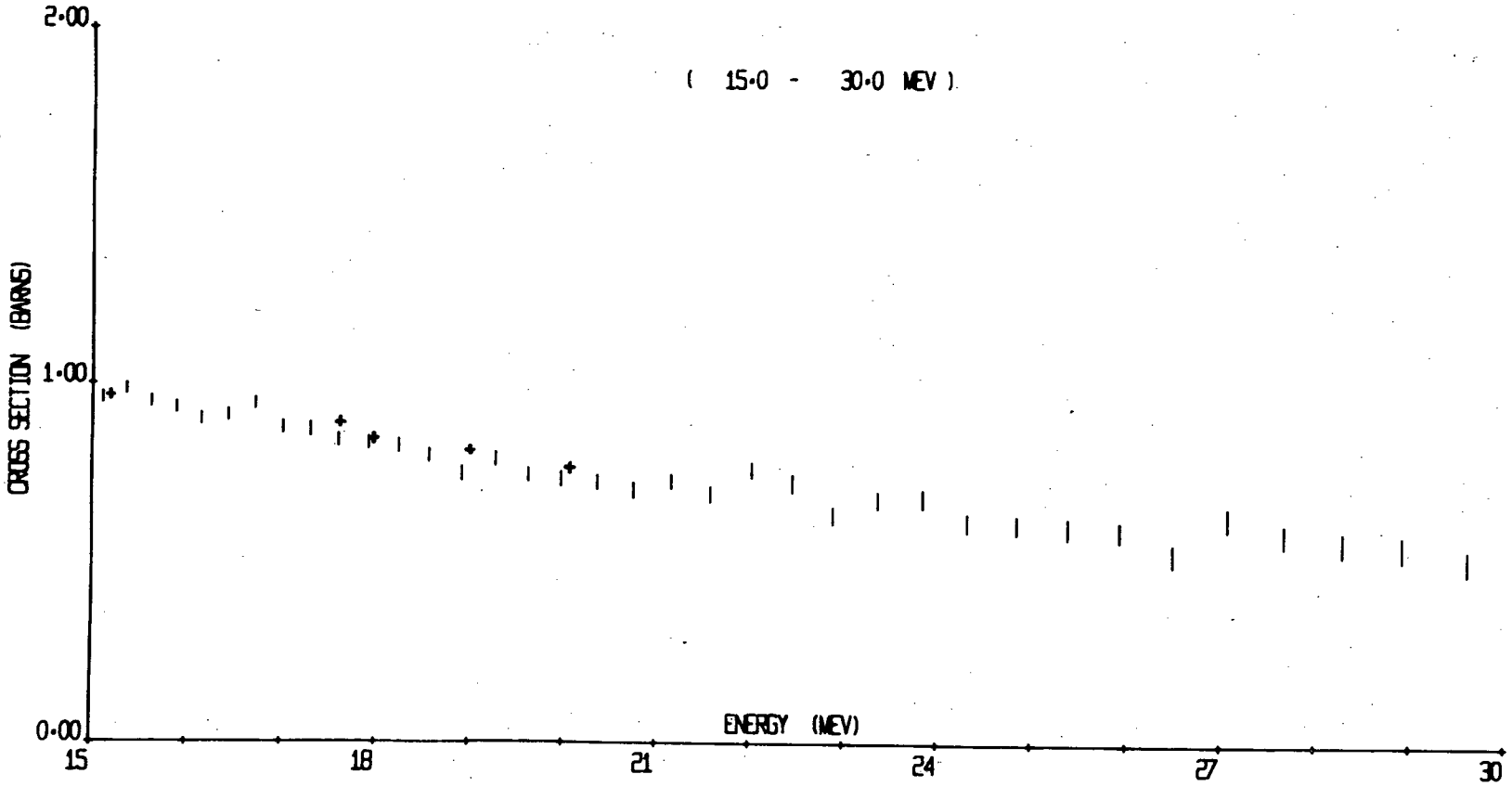
(15·0 - 30·0 MEV)
CROSS SECTION (BARNS)
2·00
1·00
0·00
ENERGY (MEV)
15
18
21
24
27
30

Figure 4

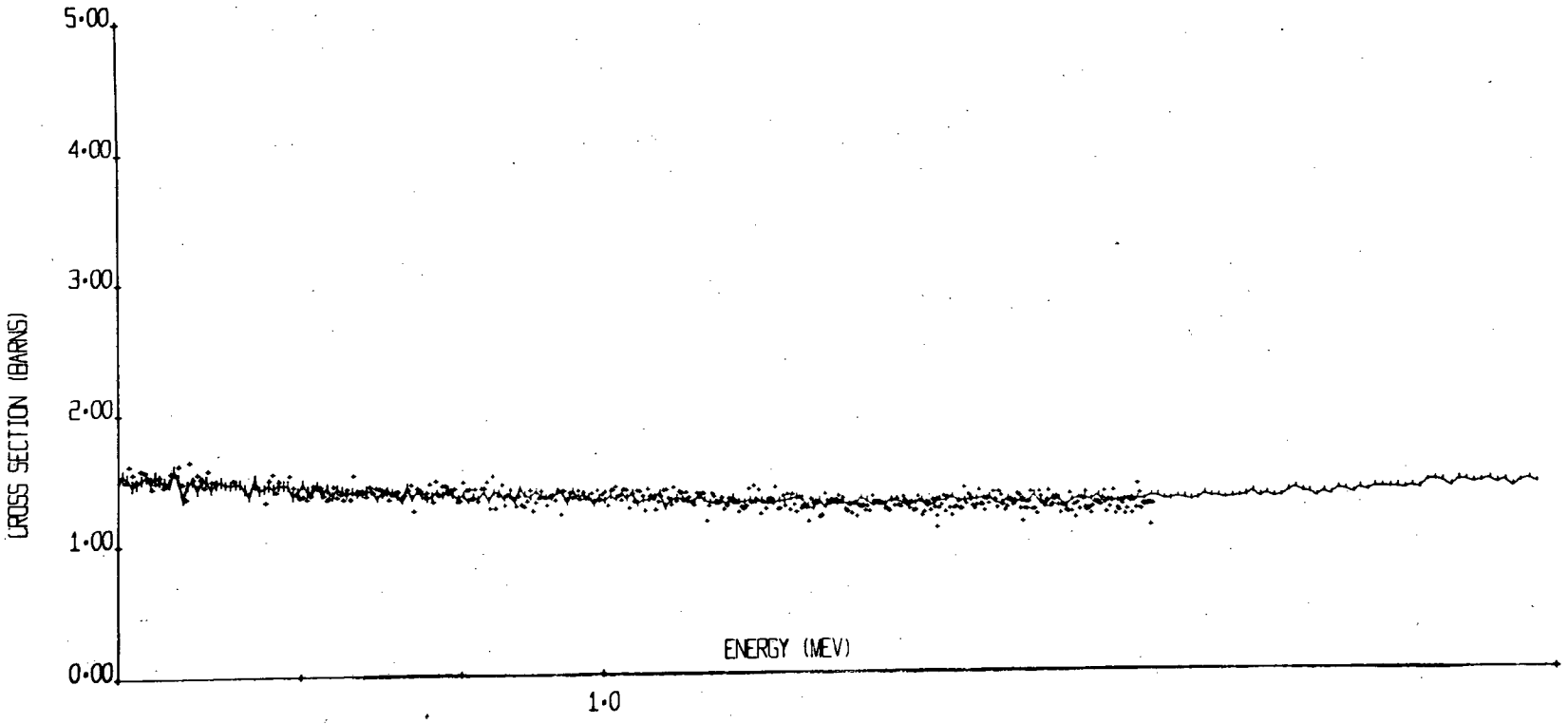

Figure 5

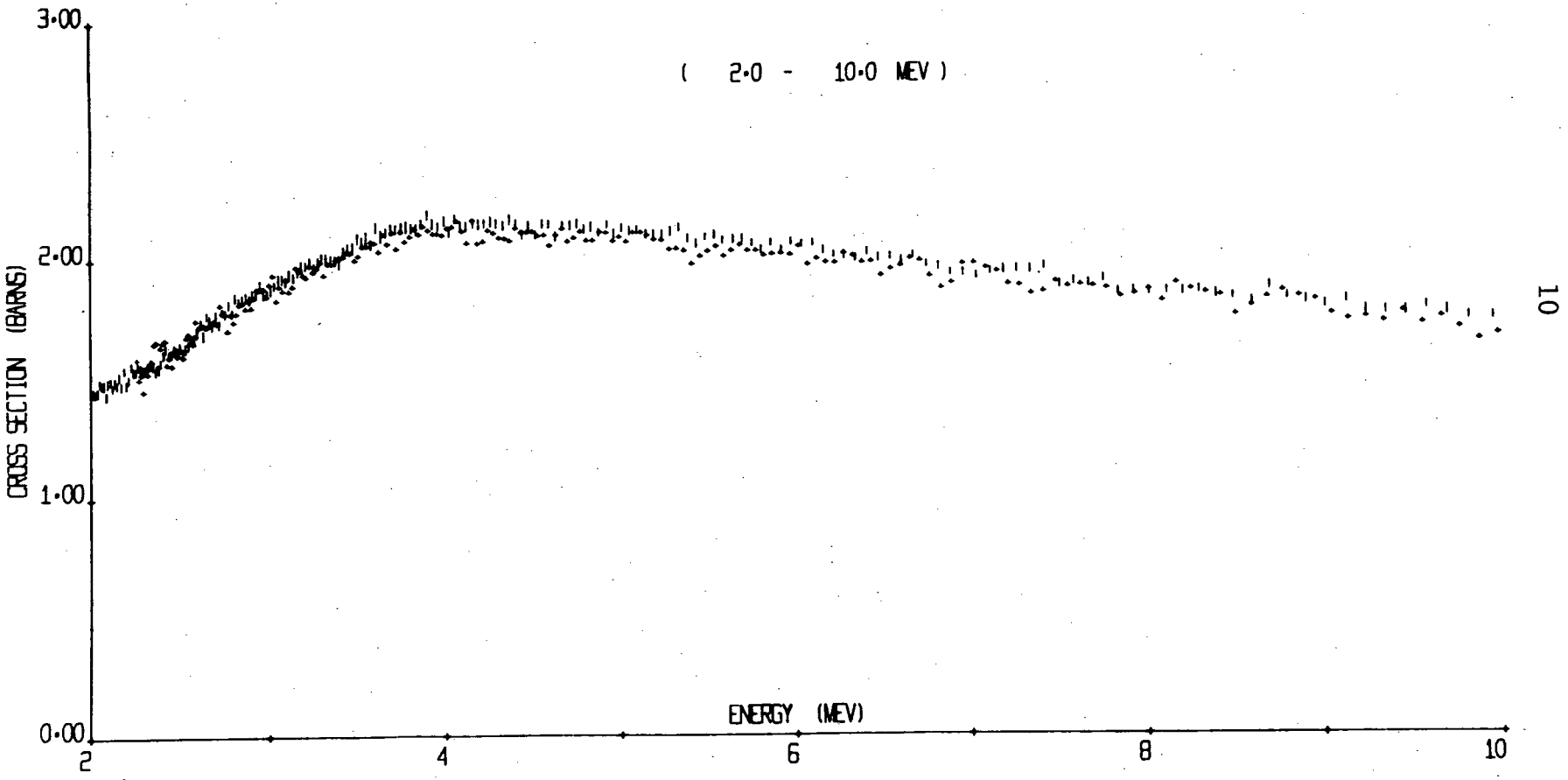
(2·0 - 10·0 MEV)
CROSS SECTION (BARNS)
3·00
2·00
1·00
0·00
2
4
6
8
10
ENERGY (MEV)
10

Figure 6

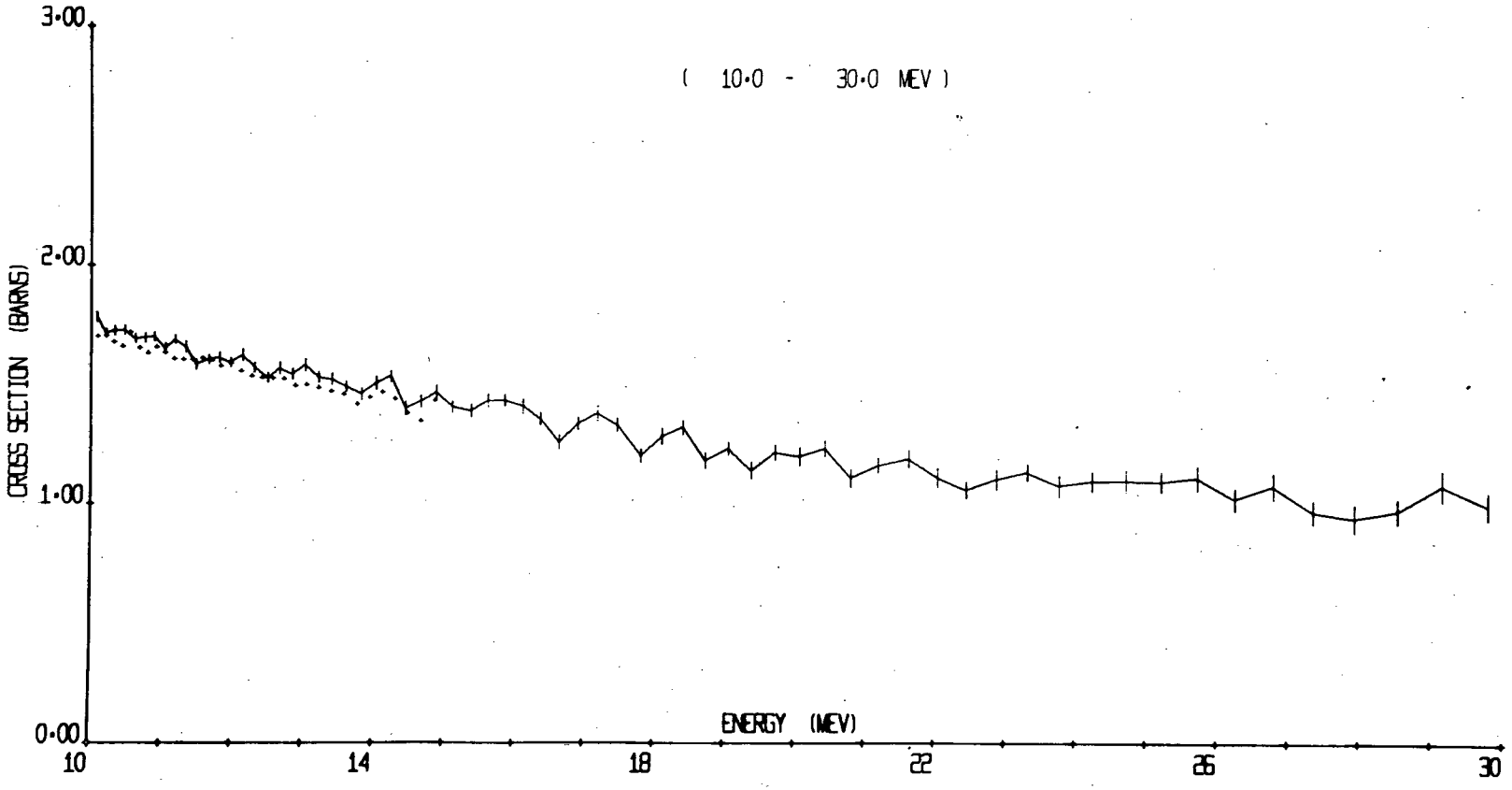
(10·0 - 30·0 MEV)
CROSS SECTION (BARNS)
3·00
2·00
1·00
0·00
ENERGY (MEV)
10
14
18
22
26
30

Figure 7

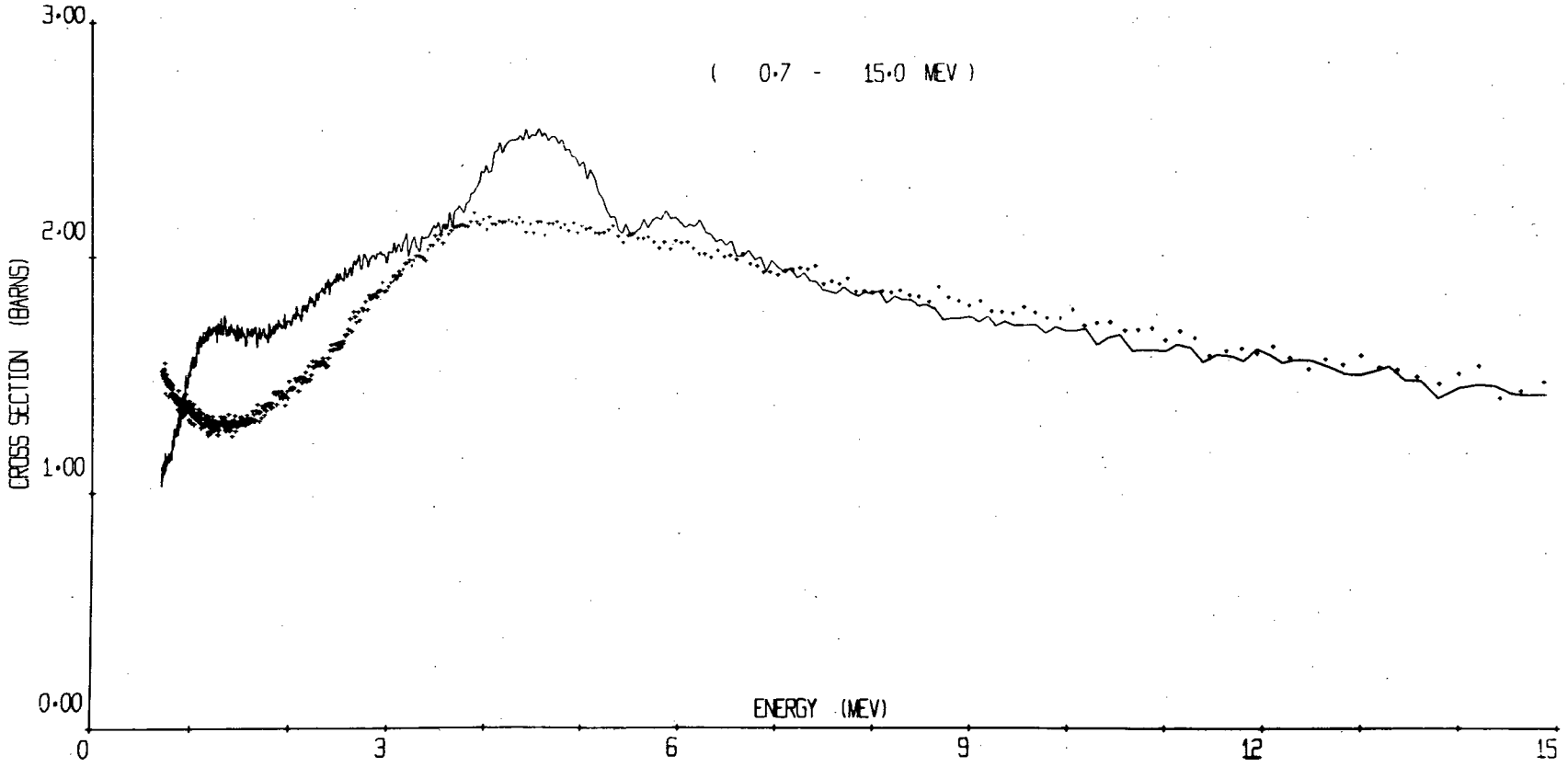
(0·7 - 15·0 MEV)
CROSS SECTION (BARNS)
3·00
2·00
1·00
0·00
ENERGY (MEV)
0
3
6
9
12
15

Figure 8

IRON-FILTERED NEUTRON BEAMS - A NEW APPROACH TO PRECISION TIME-OF-FLIGHT CROSS-SECTION MEASUREMENTS

R. C. Block, N. N. Kaushal and R. W. Hockenbury

The following is a report accepted for presentation at the National Topical Meeting of the American Nuclear Society at Kiamesha Lake, New York, September 12-15, 1972.

1. Introduction

By placing thick filters in a white-source time-of-flight neutron beam, it is possible to obtain a low-background transmitted beam of bands of neutrons with energies corresponding to the cross-section minima in the filter. Iron filters varying in thickness from 2 to 20 inches were placed in the 25-meter spectrometer of the RPI LINAC, and, for filters 6 inches and thicker, over ten distinct neutron energy bands were observed below 1 MeV. In particular, the band at 24.3 keV is ~2.4 keV wide and is separated by more than 45 keV from the next nearest energy band. In the upper half of Fig. 1 are plotted (as a function of neutron time-of-flight) the relative neutron intensities near 24.3 keV for neutrons filtered by 2, 8, 14 and 20 inches of 'pure' Armco iron. A ^{10}B-NaI detector (as described in Refs. 1 and 2) was used for this measurement. For the thicker filters, the peak counting rate is about 500 times greater than background (as measured in the wings), and this small background can readily be determined, permitting high accuracy cross-section measurements near 24.3 keV. Measurments using this technique have already been reported[3] up to ~1 MeV for the total cross section of iron near the resonance-interference minima.

2. Capture Measurements

For capture cross-section measurments an 8-inch thickness of iron was selected for the filter and a 1.25-meter liquid scintillator capture detector[1,2] was used to detect neutron captures. Since the 24.3 keV window is ~2.4 keV wide, high resolution is

not necessary to define this region. Therefore, the LINAC was operated with a rather wide burst width of 0.5 μsec to obtain 12 to 15 kw of beam power on the electron target. The beam energy was approximately 60 MeV and the repetition rate was 500 pps. A representative set of capture data is shown in the lower half of Fig. 1 for two relatively short runs. The gamma ray bias on the detector was set from 3 to 15 MeV for these data. The high peak-to-background ratios of 46:1 for Ta and 9:1 for U provide an ideal low-background environment for capture measurements with a minimum of time-dependent background effects (caused by neutrons scattered into the scintillator.

In particular, the background on either side of the iron window seems quite flat and suggests that the background in the region of the window is also flat. However, it was also possible that the background under this curve could have structure near the window, so it was necessary to measure this directly. A 3-inch thick sample of reactor-grade graphite was placed in the capture detector to scatter essentially 100% of the filtered neutron beam into the detector. Since the carbon capture cross section is less than 1 millibarn, any structure in the counting rate near 24.3 keV would be due to the prompt* scattering sensitivity of the detector. This sensitivity was measured to be $5.5 \pm 0.8 \times 10^{-5}$ false capture counts per scattered neutron at a bias of 3 to 15 MeV, and about 8×10^{-5} at a bias of 2 to 15 MeV. Reference 1 reported a value of 1×10^{-5} for 3 to 15 MeV bias at a neutron energy of ~85 keV. This result assumed that the ^{24}Mg radiation width at 85 keV is ~1 eV. If the revised value[4] of 4 ± 1 eV is taken for the radiation width, the scattering sensitivity at 85 keV becomes $(4 \pm 1) \times 10^{-5}$, in excellent agreement with the 24.3 keV filtered beam value of $(5.5 \pm 0.8) \times 10^{-5}$.

*By prompt scattering sensitivity is meant the detection of scattered neutrons within several tens of nanoseconds after the scattering, as contrasted to neutrons which thermalize in the liquid and lead to detected events tens of microseconds later.

3. Analysis of Capture Data

The capture counts C_i from samples, integrated over the 24.3 keV neutron energy band, is

$$C_i = \int_{\sim 24.3 \text{ keV}} \eta_i \, Y_i(E) \, \phi(E) dE \qquad (1)$$

where

η_i ≡ capture detector efficiency

$Y_i(E)$ ≡ capture yield (or captures per incident neutron upon the sample) at energy E

$\phi(E)$ ≡ number of neutrons incident upon the sample, per unit neutron energy, at energy E

If the sample is thin, the yield $Y_i(E)$ is approximately equal to $N_i \sigma_{\gamma i}(E)$, where N_i is the sample thickness and $\sigma_{\gamma i}(E)$ in the capture cross section at energy E. Thus, for thin samples, Eq. (1) reduces to

$$C_i \approx \int_{\sim 24.3 \text{ keV}} \eta_i \, N_i \sigma_{\gamma i}(E) \, \phi(E) dE \approx \eta_i \, N_i \int_{\sim 24.3 \text{ keV}} \sigma_{\gamma i}(E) \, \phi(E) dE \, , \qquad (2)$$

where the capture detector efficiency is assumed constant over the 24.3 keV energy band.

We can define the effective cross section $\tilde{\sigma}_{\gamma i}$ as

$$\tilde{\sigma}_{\gamma i} \equiv \frac{\int \sigma_{\gamma i}(E) \, \phi(E) dE}{\int \phi(E) dE} \qquad (3)$$

and then Eq. (2) reduces to

$$C_i \approx \eta_i \, N_i \tilde{\sigma}_{\gamma i} \int \phi(E) dE \, . \qquad (4)$$

The effective cross section $\tilde{\sigma}_{\gamma i}$ is the integral of the capture cross section over the flux distribution of the 24.3 keV energy band. If the capture cross section is constant or slowly varying in this interval, $\tilde{\sigma}_{\gamma i}$ represents the average capture cross section near 24.3 keV.

4. Relative $\tilde{\sigma}_\gamma$ for In, Ta, Au and ^{238}U

In order to measure the relative cross section $\tilde{\sigma}_\gamma$ for In, Ta, Au and ^{238}U (depleted to 0.2% ^{235}U), it is necessary to measure (1) the relative capture counting rate C_i from thin samples of these elements and (2) the relative capture detector efficiency η_i for each sample. The relative capture rates were measured by alternating samples of In, Ta, Au and ^{238}U (99.8%) into the capture detector for two to three minute intervals over a total time of sixteen hours. The operating bias was set from 2 to 15 MeV. The sample thicknesses and net capture counts (corrected for background) are listed in Columns (2) and (3) of Table I. The errors shown in Column (3) represent standard deviations based on counting statistics.

In principle, the detector efficiency η_i is equal to the product of the cascade efficiency and the spectrum fraction. The cascade efficiency is the probability that the capture event will deposit some energy in the capture detector so that, in principle, with zero operating bias, it can be detected. The spectrum fraction is that fraction of the total detectable events which are passed by the operating bias. For In, Ta, Au and ^{238}U, the cascade efficiencies differ by less than 1% and can be ignored in a relative measurement. The spectrum fractions are determined by (1) measuring the capture pulse-height distributions for ~24.3 keV capture, (2) extrapolating the distributions to zero bias and (3) calculating the fraction of capture events which are passed with the operating bias. These spectra are plotted in Fig. 2 along with three linear extrapolations from zero to 1.8 MeV: (a) a 'best given' extrapolating, and (b) and (c) 'extreme' estimates of the extrapolation. From these spectra, the spectrum fractions were obtained for the operating bias of 2 to 15 MeV; these results are tabulated in Columns (4), (5) and (6) in Table I. For Au, In and Ta, the (b) and (c) spectrum fraction

do not differ from the (a) spectrum fraction by more than about 2 or 3%. For ^{238}U, the spectrum fraction for (c) is about 8% higher than for (a), and for (b) it is about 3% lower than for (a). Since extrapolation (c) represents an extreme case for U (see Fig. 2), in that it goes to zero pulse height at zero MeV, this is perhaps too pessimistic. Thus we regard the spectrum fraction based on extrapolation (a) to be accurate to about 5 or 6%.

The relative 24.3 keV integrated cross section $\sigma_{\gamma,i}$ was determined by applying Eq. (4) to the data in Columns (2), (3) and (4) of Table I. However, there were multiple scattering and sample attenuation effects which amounted to several percent corrections to these data. The analysis of Schmitt[5] was used to correct these results; these corrections are listed in Column (7). The results are expressed in Column (8) as the ratio to the Au effective cross section. The samples were sufficiently thin (95 to 99% transmission) so that thick-sample corrections are less than a few percent. Poenitz[6] estimates the Au average capture cross section to be 600 mb at 30 keV, which extrapolates to 667 mb at 24.3 keV. Assuming that the Au average cross section is equal to the effective cross section, the results in Column (8) can be normalized to the Au cross section; these results are listed in Column (9).

The ratio of effective cross sections in Column (8) is estimated to be accurate within 3 to 5%. However, the effect of local fluctuations in the cross section caused by the nuclear statistics must be taken into account before any accurate comparisons can be made with the wealth of low-resolution average capture cross section data near 24.3 keV; e.g., in the case of ^{238}U, the average level spacing for s-wave resonances is ~16 eV and ~5.3 eV for p-wave resonances. Thus, in the ~2.4 keV wide energy band near 24.3 keV, there are on the average ~150 s-wave levels and ~450 p-wave levels. The fluctuations in the local capture cross section resulting from the finite number of levels sampled in this interval, can be as much as 5 to 7% from the average cross section

measured in a low resolution experiment. Thus, even though the filtered beam measurement is intrinsically capable of extremely high accuracy, it is necessary to couple it with high resolution, medium accuracy capture measurements to pin down the statistical fluctuations. Once this is done, these filtered beam measurements can serve as a benchmark to which the continuous energy results may be compared and normalized.

5. Conclusion

This technique has enabled the 24.3 keV relative effective cross sections of In, Ta, Au and ^{238}U to be measured with an accuracy of about 4 or 5%. This accuracy is limited primarily by the spectrum fraction uncertainty due to the extrapolation to zero pulse height. This can be improved significantly in the future by normalizing these measurements to low energy capture in black resonances (e.g., the 4.9 eV Au resonance, etc.), perhaps reducing the overall uncertainty to at most 2 to 3%. In addition, high-resolution white-source time-of-flight capture measurements must be carried out to determine the local cross-section fluctuations near 24.3 keV so that these filtered beam measurements can serve as a benchmark to which continuous energy results may be compared and normalized.

REFERENCES:

1. R. W. Hockenbury, Z. M. Bartolome, J. R. Tatarczuk, W. R. Moyer and R. C. Block, Phys. Rev., 178, 1746 (1969).
2. Z. M. Bartolome, R. W. Hockenbury, W. R. Moyer, J. R. Tatarczuk, and R. C. Block, Nucl. Sci. Eng., 37, 137 (1969).
3. R. C. Block, K. Alfieri and P. J. Turinsky, Trans. Am. Nucl. Soc., 15, 531 (1972).
4. Z. M. Bartolome, J. R. Tatarczuk, W. R. Moyer and R. C. Block, Linear Accelerator Project Progress Report, RPI-328-97, 24 (1967).
5. H. W. Schmitt, 'Sample Scattering Corrections in Neutron Beam Experiments," ORNL-2883, Oak Ridge National Laboratory (1960).
6. W. P. Poenitz, Proc. of Conf. on Neutron Standards and Flux Normalization, CONF.-701002, p. 320 (1971).

FIGURE CAPTIONS

Fig. 1 In the Upper Half of this Figure are Plotted the ^{10}B-NaI Neutron Counting Rate vs. Neutron Time of Flight for a Pulsed Neutron Beam Passing through 2, 8, 14 and 20 Inches of Iron. The peak transmission through each filter is shown in parentheses. In the lower half of this Figure are plotted the capture counting rate vs. neutron time of flight for capture in depleted U and Ta samples and with an 8-inch iron filter.

Fig. 2 Pulse Height Spectra for ~24.3 keV Neutron Capture in Samples of Au, Ta, U (depleted) and In.

RELATIVE NEUTRON INTENSITY FOR 2", 8", 14", AND 20" IRON FILTERS

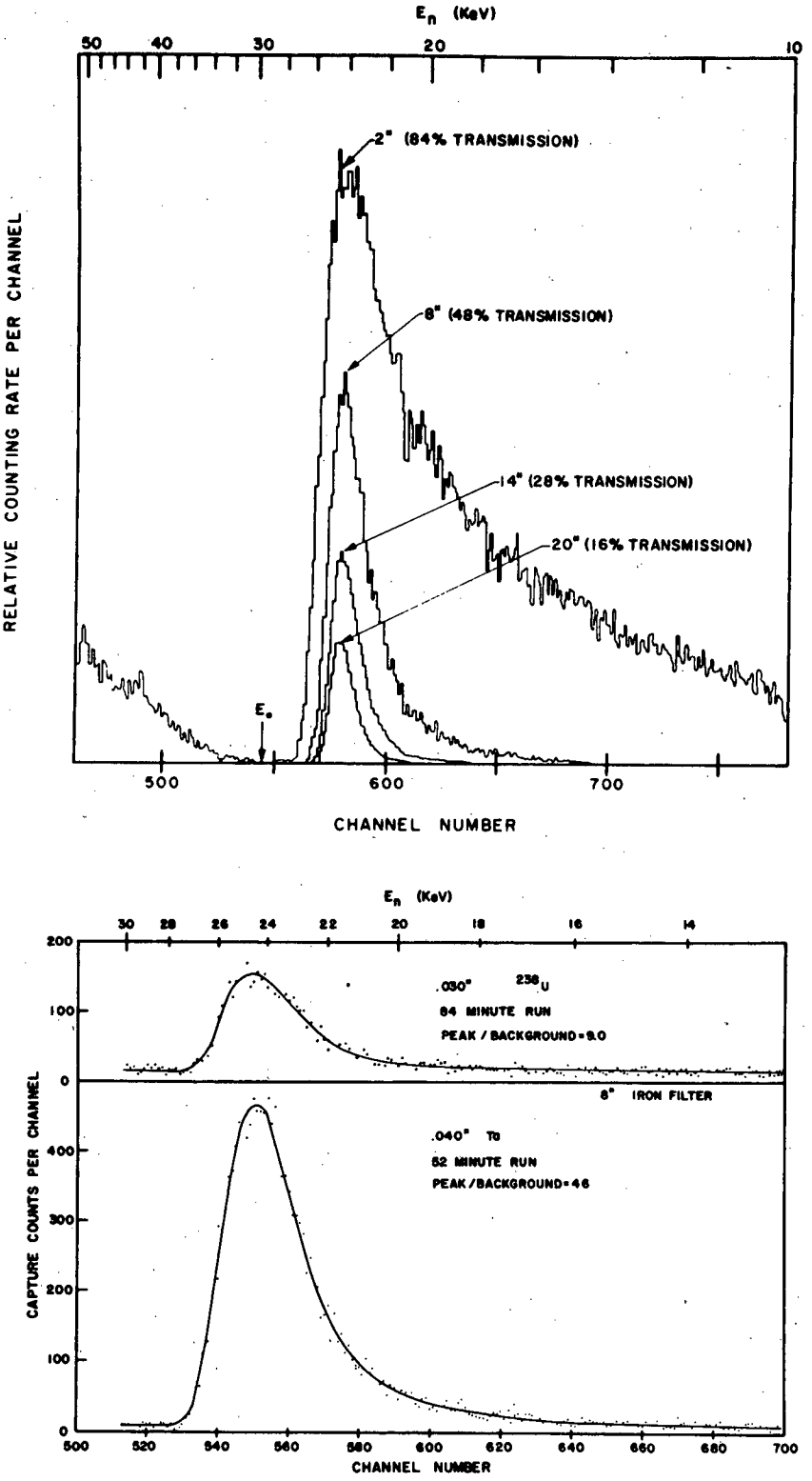

Figure 1

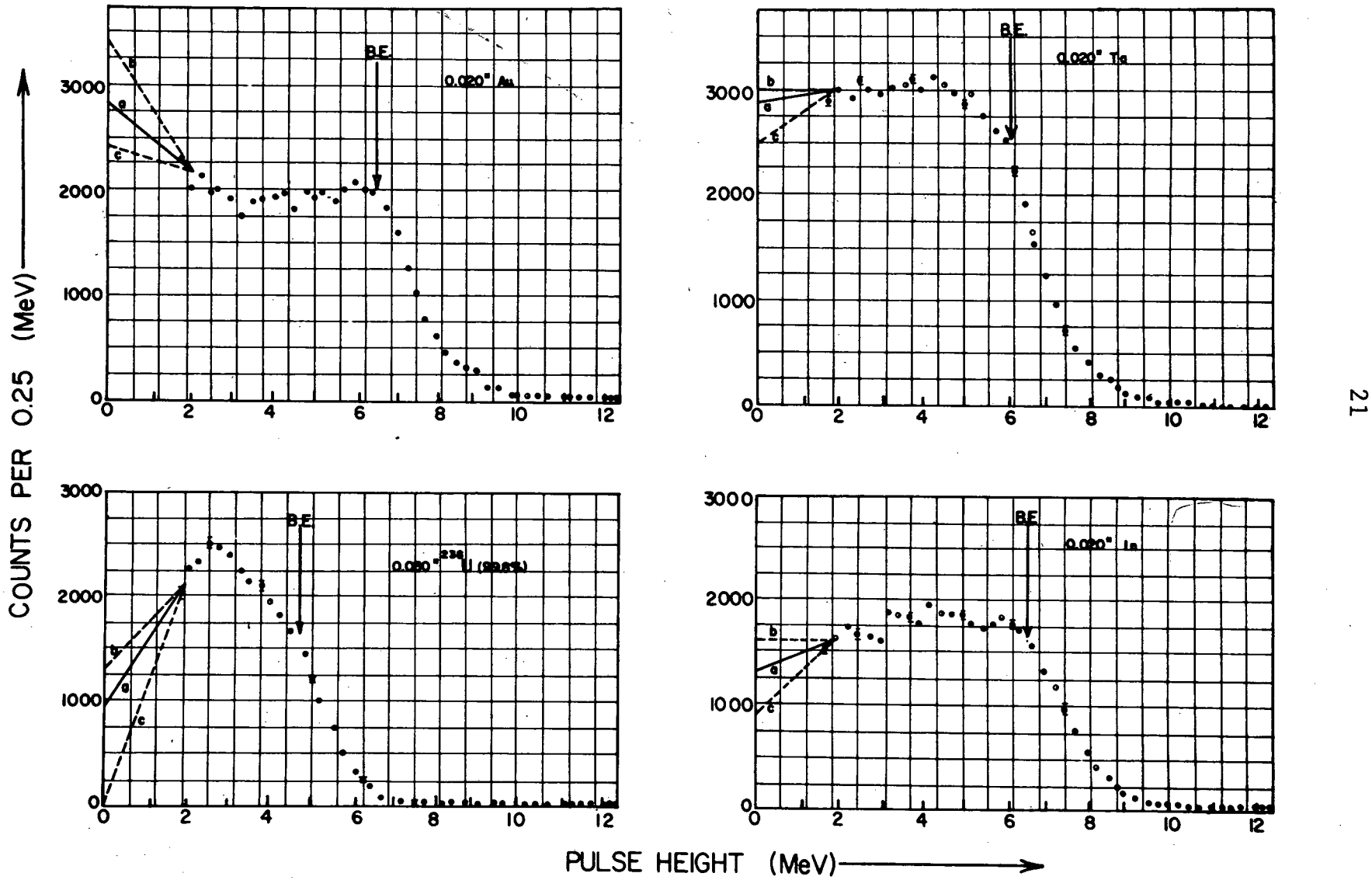
COUNTS PER 0.25 (MeV)
PULSE HEIGHT (MeV)
B.E.
0.020" Au
0.020" Ta
0.020" In
a
b
c
0
1000
2000
3000
0
2
4
6
8
10
12

Figure 2

Table I. Capture Near 24.3 KeV

Element	Thickness (10^{-3} at/bn)	Net Capture Counts		Spectrum Fraction* (a)	(b)	(c)	Sample Thickness Correction	$\tilde{\sigma}_{\gamma i}/\tilde{\sigma}_{\gamma i}$Au**	$\tilde{\sigma}_{\gamma i}$*** (barns)
Au	3.134	25,313	(+0.7%)	0.694	0.670	0.710	3.6%	(1.00)	(0.67)
In	1.964	22,990	(±0.8%)	0.777	0.761	0.798	2.2%	1.32	0.88
^{238}U(99.8%)	3.800	22,101	(±0.8%)	0.680	0.658	0.732	6.8%	0.70+	0.47+
Ta	3.104	37,586	(±0.6%)	0.714	0.709	0.725	4.9%	1.44	0.96

*See Fig. 2 for extrapolation-to-zero-pulse-height schemes (a), (b) and (c).

**Based on spectrum fraction (a).

***Assuming $\tilde{\sigma}_{\gamma i}$,Au = 670 mb.

+Corrected for ^{235}U contamination.

TEMPERATURE-DEPENDENT TRANSMISSION AND SELF-INDICATION MEASUREMENTS UPON DEPLETED U IN THE UNRESOLVED REGION[+]

T. Y. Byoun,[*] R. C. Block and T. Semler[#]

The following is a report accepted for presentation at the National Topical Meeting of the American Nuclear Society at Kiamesha Lake, New York, September 12-15, 1972.

1. Experimental Technique

A series of neutron average transmission and self-indication ratio measurements have been made at the RPI LINAC on depleted U (99.8% ^{238}U, and 0.2% ^{235}U) up to 100 keV in order to investigate the temperature dependence of resonance self-shielding in the unresolved energy region. These measurements were carried out at 77°K, 295°K and 973°K. Five sample thicknesses (0.00758, 0.01552, 0.03155, 0.04670 and 0.06206 atom/barn) have been used for the room temperature measurements. Samples of 0.03155 atom/barn and of 0.06206 atom/barn have been used for the temperature-dependent measurements. A thin self-indication sample of 0.00376 atom/barn has been kept inside the capture detector at room temperature throughout the self-indication experiments. The experimental method has been described in detail in a previous publication on Ta,[1] except that a vacuum furnace was used in this experiment instead of the argon-flow furnace.

The experimental results are plotted in Fig. 1. The data have been averaged in 10% wide energy bins. The statistical accuracy of the data is approximately 1% for the transmission and approximately 2% for the self-indication ratios. Sample thicknesses indicated in Fig. 1 are actual sample thicknesses measured at the corresponding temperatures. The linear thermal expansion coefficient of the U sample was measured to be $(1.7 \pm 0.1)\%$ between 295°K and 973°K, and $-(0.20 \pm 0.02)\%$ between 295°K and 77°K.

[+]Work supported by NASA Grant NGR 33-018-134.

[*]Based in part on the Ph.D. Thesis of T. Y. Byoun.

[#]NASA Lewis Research Center, Cleveland, Ohio 44135.

2. Analysis

The average cross section and strength functions for s- and p-wave neutrons in the energy range 1 keV to 70 keV and the limited range 5.0 to 5.6 keV have been determined by using the least squares method. A stochastic sampling method using the computer code DAISY[1,2] was used to analyze the temperature-dependent transmission data in the energy range 5.0 keV to 5.6 keV. The results and the parameters used are listed in Table I.

An analytical calculation also has been performed to analyze the data by averaging combinations of resonance parameters over corresponding distribution functions. The expressions for the average transmission, <TR>, and for the self-indication ratio, <SIR>, have been approximated by expanding the exponential in the average transmission and in the self-indication ratio to four terms as

$$\langle TR\rangle = e^{-n\langle\sigma_t\rangle}\left\{1+\tfrac{1}{2}n^2\langle(\sigma_t-\langle\sigma_t\rangle)^2\rangle - \tfrac{1}{6}n^3\langle(\sigma_t-\langle\sigma_t\rangle)^3\rangle\right\} \quad (1)$$

$$\langle SIR\rangle = \frac{e^{-n\langle\sigma_t\rangle}}{\langle\sigma_\gamma\rangle}\left\{\langle\sigma_\gamma\rangle - n\langle\sigma_\gamma(\sigma_t-\langle\sigma_t\rangle)\rangle + \tfrac{1}{2}n^2\langle\sigma_\gamma(\sigma_t-\langle\sigma_t\rangle)^2\rangle - \tfrac{1}{6}n^3\langle\sigma_\gamma(\sigma_t-\langle\sigma_t\rangle)^3\rangle\right\} \quad (2)$$

where <...> stands for the average over an energy interval, ΔE, and n is the sample thickness in units of atom/barn. The other notations are explained in Table II.

The following assumptions have been used in the analytical calculation:

1. The Wigner level spacing distribution and the Porter-Thomas width distribution function are valid.

2. Level spacing between levels with same spin J and orbital angular momentum ℓ, $D_{\ell J}$, is assumed to have only J-dependence. The radiation width, $\Gamma_{\gamma\ell}$, is treated as a constant. The inelastic neutron width is considered constant above the inelastic threshold.

3. The energy interval, ΔE, over which cross sections or resonance parameters are averaged is assumed to be large enough to contain a statistically meaningful number of resonances, yet small enough to treat the slowly varying parameters (such as wave length) as constant in ΔE.

4. Level-level interference effects other than those caused by mere overlap of Breit-Wigner resonances are neglected.

5. The Lamb effective temperature theory[5] for the Doppler broadened cross section is valid.

The analytical method is applied by assuming a set of strength functions, S_ℓ, average level spacings, $\langle D_\ell \rangle$, nuclear radius, R, and the sample temperatures, T. The effective temperature[5,6] T_{eff}, the average reduced neutron width for the (ℓ,J)-channel, $\langle \Gamma_{nJ}^{\ell} \rangle$, and $\langle D_{\ell J} \rangle$ are calculated using the following:

$$T_{eff}/T = 1 + \frac{1}{20}(\theta/T)^2 - \frac{1}{1680}(\theta/T)^4 + \frac{1}{90720}(\theta/T)^6 \qquad (3)$$

$$\langle D_{\ell J} \rangle = \langle D_\ell \rangle \sum_{J'} g_{J'}/g_J \qquad (4)$$

$$\langle \Gamma_{nJ}^{\ell} \rangle = \langle D_{\ell J} \rangle S_\ell \quad , \qquad (5)$$

where g_J = statistical spin factor of resonance of spin J, and T_{eff}=Debye temperature. Then various average quantities such as the average of the total and capture cross sections, the variance and the covariance of the cross sections, and the triance and the cotriance are calculated. The average transmission and self-indication ratio are calculated with these average quantities for the different sample thicknesses and temperatures. These calculated results are compared with the experimental values and the absolute difference between calculated values, R^{cal}, and experimental values, R^{exp} (weighted by the standard error of the experimental values, ΔR^{exp}), is determined as follows:

$$\Delta R = \frac{| R^{exp} - R^{cal} |}{\Delta R^{exp}} \qquad (6)$$

The average input parameters are then iteratively varied until the expression in Eq. (6) is minimized. The final results are tabulated in Tables III, IV and V.

3. Results and Discussion

The average resonance parameters that best fit the experimental data are listed in Table IV. Typical results of sample thickness dependence of the average transmission and self-indication ratios are shown in Fig. 2. For a given temperature (295^{o}K) and for a given neutron energy (22.63 keV to 25.02 keV), the sample thickness has been varied from 0.001 atom/barn to 0.1 atom/barn. In Fig. 3, the temperature dependence of the average transmission and self-indication ratios are shown for a given sample thickness (0.03155 atom/barn) and for a given energy range (22.63 - 25.02 keV) over a temperature range from 77^{o}K to 1000^{o}K. Experimental values are shown on both these Figures. Figure 3 shows that the average transmission decreases as temperature increases; however, the self-indication ratio increases as temperature increases. These opposite characteristics are due to the fact that in this energy range, the average transmission is governed mainly by the wings of the resonance; whereas the self-indication ratio emphasizes the cross section near the resonance peaks.

The calculated results are in good agreement with experiments in the energy range 15 keV to 100 keV, as can be seen in Tables III and IV. However, the four-term expansion of the exponential in Eqs. (1) and (2) is inadequate for cases where $n\sigma_t$ becomes large. This occurs at low energies for thick samples, and for low temperature, where peak cross sections are enchanced. This 'breakdown' of the four-term approximation is apparent in Table III. For example, in the energy range 10.16 to 11.23 keV, the low temperature and thick sample calculated results are in very poor agreement with the experimental results.

CONCLUSION

The average parameters which fit these data in the unresolved resonance region are in essential agreement with the extrapolation of the resolved resonance region average parameters. However, this

experiment sheds light on local fluctuation of these parameters. The four-term expansion analytical approach is well suited for fitting the higher energy measurements, and it serves as a starting point for stochastic methods of treating the data.

REFERENCES:

1. T. Y. Byoun, R. C. Block and T. Semler, 3rd Neutron Cross Sections and Technology Conference, CONF.-710301, Vol. 2 (1970).
2. T. Semler, The DAISY Program, NASA TND-5827.
3. L. B. Miller, W. P. Poenitz, Nucl. Sci. Eng., 35, No. 2 (1969).
4. Linear Accelerator Project Progress Report, January - March 1970, RPI-328-187.
5. W. E. Lamb, Jr., Phys. Rev., 55, 190 (1939).
6. C. M. Fleck and H. A. Weisshaupl, Nucl. Inst. and Methods, 61 (1968).
7. N. Rosenweig and C. E. Porter, Phys. Rev., 120, 1698 (1960).

FIGURE CAPTIONS

Fig. 1-A and B — Average Transmission and Self-Indication Ratio Measured for 5 Samples of Uranium.

Fig. 2 — Sample Thickness Dependence of the Average Transmission and Self-Indication Ratios.

Fig. 3 — Temperature Dependence of the Average Transmission and Self-Indication Ratios.

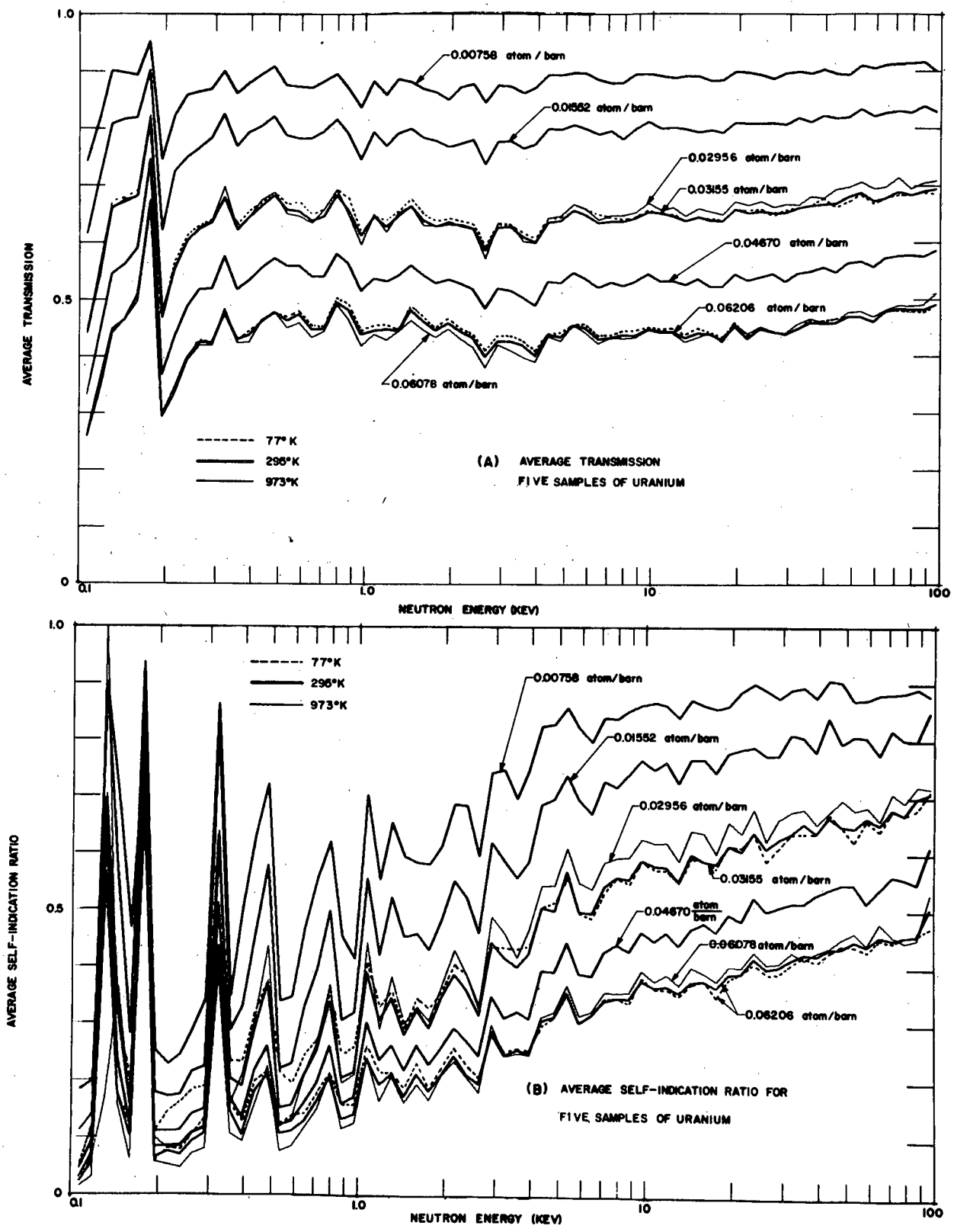
1.0
0.5
0
AVERAGE TRANSMISSION
0.00758 atom / barn
0.01552 atom / barn
0.02956 atom / barn
0.03155 atom / barn
0.04670 atom / barn
0.06206 atom / barn
0.06078 atom / barn
77° K
296°K
973°K
(A) AVERAGE TRANSMISSION
FIVE SAMPLES OF URANIUM
0.1
1.0
10
100
NEUTRON ENERGY (KEV)
AVERAGE SELF-INDICATION RATIO
(B) AVERAGE SELF-INDICATION RATIO FOR
FIVE SAMPLES OF URANIUM

Figure 1

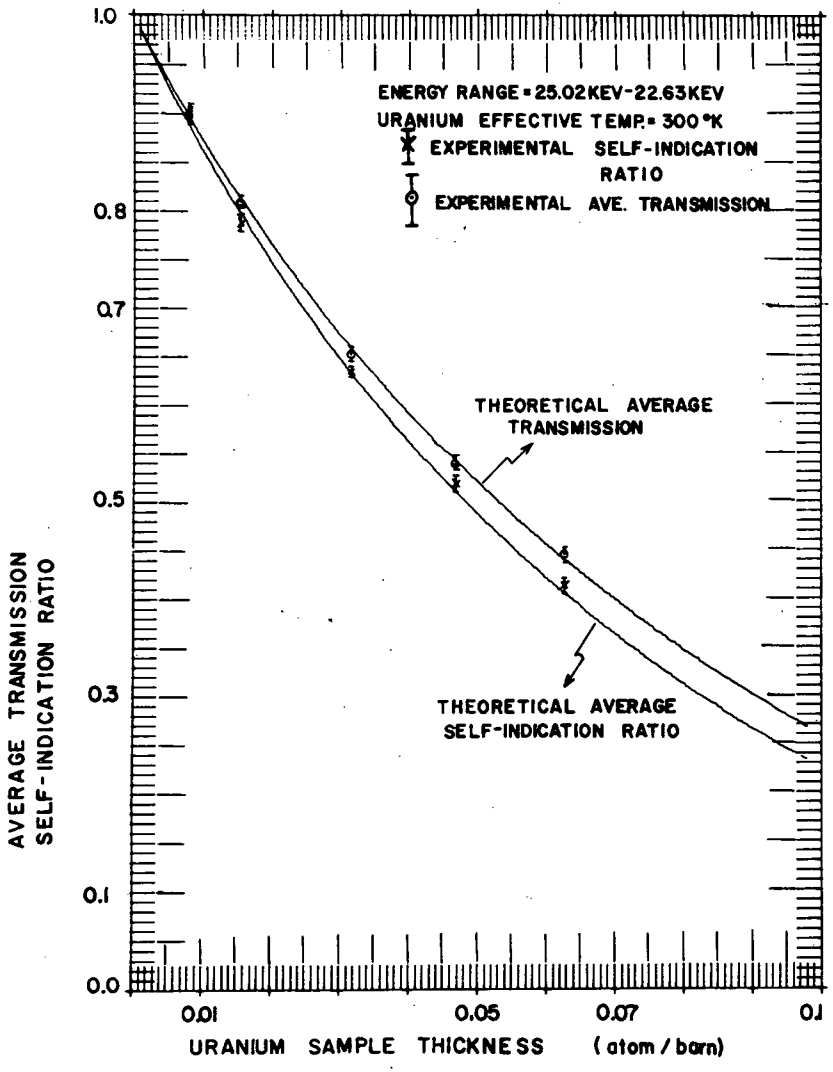

Figure 2

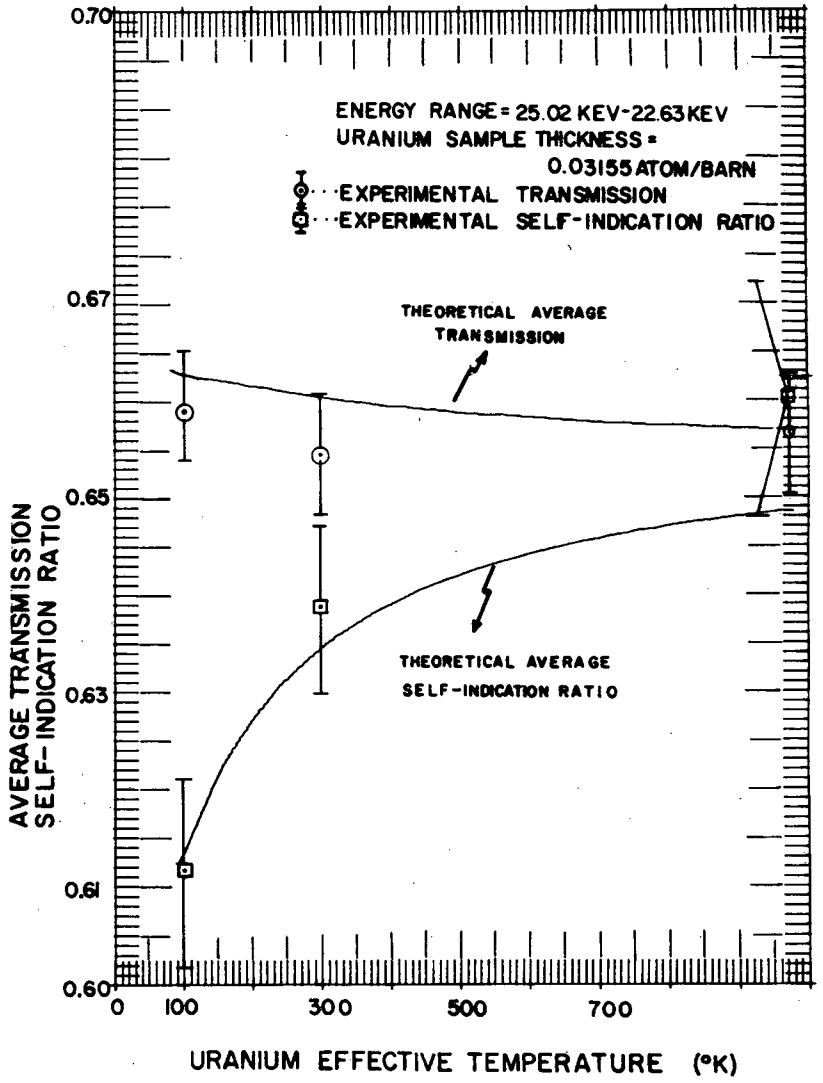

Figure 3

Table I. TRANSMISSION DATA ANALYSIS

Sample[a] Thickness (atom/barn)	Sample Temp. (°K)	Energy Range 5.0 to 5.6 keV: Effective Ave. Cross Section[4] (barns) — Experimental	Analytical[e] Calculation	DAISY Code[c] Calculation	Parameters used in the DAISY Code	Energy Range 1 to 70 keV: Strength Functions[d],[e] determined from Analytical Calculation
0.03155	77	12.8 ± 0.3		12.70	$S_o^{(b)} = 0.35 \times 10^{-4}$	$S_o = (0.91 \pm 0.12) \times 10^{-4}$
0.03155	295	13.3 ± 0.2	13.33	12.91	$D_s = 17.8$ eV	
0.03060	973	12.8 ± 0.3		13.11	$\sigma_p = 10.0$ barn	$S_1 = (2.3 \pm 0.6) \times 10^{-4}$
0.06206	77	12.6 ± 0.3		12.39	$\Gamma_\gamma = 0.023$ eV	
0.06206	295	12.7 ± 0.1	12.71	12.62	Debye Temp. = 200°K	
0.06292	973	12.6 ± 0.1		12.88		

(a) Measured at 295°K

(b) Local value of S_o in the energy range 5.0 keV to 5.6 keV

(c) Doppler broadening of p-wave resonance has not been considered

(d) For a given potential cross section of 10.8 barn[3] and the formula used is:

$$\langle\sigma\rangle = 2\pi^2 \lambda\lambda_1 \sum_{\ell=0}^{1} (2\ell+1) S_\ell \upsilon_\ell \cos 2\xi_\ell + \sigma_p$$

(e) Least squares fit by using the following approximate formula:

$$\langle T\rangle = e^{-n_i \langle\sigma_t\rangle} \{1 + \tfrac{1}{2} n_i^2 (\sigma_t - \langle\sigma_t\rangle)^2 \rangle - \tfrac{1}{6} n_i^3 \langle(\sigma_t - \langle\sigma_t\rangle)^3\rangle\}$$

Table II

SOME EXAMPLES OF THE ANALYTICAL FORMULAS

The average total cross section; $\langle\sigma_t\rangle$:

$$\langle\sigma_t\rangle = \frac{2\pi^2}{k_1 k} \sum_{\ell}(2\ell+1)\, V_\ell S_\ell \cos 2\xi_\ell + \sigma_p \quad . \tag{II-1}$$

The average radiative capture cross section, $\langle\sigma_\gamma\rangle$:

$$\langle\sigma_\gamma\rangle = \frac{2\pi^2}{k^2} \sum_{\ell,J} \frac{\Gamma_{\gamma\ell}}{\langle D_{\ell J}\rangle}\, g_J \left\langle\frac{\Gamma_n}{\Gamma}\right\rangle_{\ell,J} \tag{II-2}$$

, where $\left\langle\frac{\Gamma_n}{\Gamma}\right\rangle_{\ell,J} = 1 - \psi[0, \sqrt{\frac{2(\Gamma_n + \Gamma_{\gamma\ell})}{\langle\Gamma_n\rangle_{\ell,J}}}]$, for I = 0

The variance of total cross section, $\langle(\sigma_t - \langle\sigma_t\rangle)^2\rangle$:

$$\langle(\sigma_t-\langle\sigma_t\rangle)^2\rangle = \frac{2\pi^{7/2}}{2k^4\Delta} \sum_{\ell,J} g_J^2 \langle\Gamma_n\rangle^2_{\ell,J} \frac{1}{\langle D_{\ell J}\rangle} \left\{1+\left\langle\exp\left(-\frac{D^2_{\ell J}}{2\Delta^2}\right)\right\rangle_{Wig}\right\}$$

$$+ \frac{4\pi^{7/2}}{\sqrt{2}\Delta k^4} \sum_{\mu\neq\nu} g_\mu g_\nu \frac{\langle\Gamma_{n\mu}\rangle\langle\Gamma_{n\nu}\rangle}{\langle D_{\mu\nu}\rangle} \left\langle\exp\left[-\frac{D^2_{\mu\nu}}{2\Delta^2}\right]\right\rangle_{Super}$$

$$\cdot(\cos 2\xi_\mu \cos 2\xi_\nu + \sin 2\xi_\mu \sin 2\xi_\nu) + 2\langle\sigma_t\rangle\sigma_p - \sigma_p^2 \quad .$$

(II-3)

Notations used above are:

k = neutron wave number,

ξ_ℓ = potential scattering phase shift for angular momentum ℓ,

σ_p = potential scattering cross section = $\frac{4\pi}{k^2}\sum_{\ell}(2\ell+1)\sin^2\xi_\ell$,

V_ℓ = hard sphere penetration factor,

Δ = Doppler width,

$\left\langle\frac{\Gamma_n}{\Gamma}\right\rangle_{\ell,J}$ = Porter-Thomas width distribution average of $\left(\frac{\Gamma_n}{\Gamma}\right)_{\ell,J}$,

$\langle\cdots\rangle_{Wig}$ = Wigner level spacing distribution average,

$\langle\cdots\rangle_{Super}$ = Average over the double populationed (with different spin state) Wigner distribution,

ψ = Doppler function difined as $\psi(x,\theta) = \frac{\theta}{2\sqrt{\pi}} \int_{-\infty}^{\infty} \frac{\exp[-\frac{\theta^2}{4}(x-y)^2]}{1+y^2}\, dy$

with standard notations.

The subscripts in eq. (II-3) are:

$\mu = \mu(\ell,J)$, $\nu = \nu(\ell,J)$.

The triance, $\langle(\sigma_t-\langle\sigma_t\rangle)^3\rangle$, covariance, $\langle\sigma_\gamma(\sigma_t-\langle\sigma_t\rangle^2\rangle$, and catriance term $\langle\sigma_\gamma(\sigma_t-\langle\sigma_t\rangle)^3\rangle$ can be expressed also as functions of resonance parameter statistics.

TABLE III

RESULTS OF ANALYTICAL CALCULATION COMPARED WITH EXPERIMENTAL RESULTS[a]

ENERGY RANGE(EV)=91893.-83141. TOTAL=12.507 CAPTURE=0.2316

AT/BARN	TEFF	TR-OBS	ETR-OB	TR-CAL	SIR-OB	ESR-OB	SIR-CA
0.00758	301.	0.9146	0.0077	0.9098	0.8932	0.0179	0.9108
0.01552	301.	0.8377	0.0070	0.8248	0.7998	0.0161	0.8261
0.03155	301.	0.6887	0.0059	0.6782	0.7006	0.0142	0.6788
0.04670	301.	0.5744	0.0050	0.5653	0.5485	0.0115	0.5640
0.06206	301.	0.4808	0.0043	0.4712	0.4580	0.0098	0.4675
0.02956	975.	0.7048	0.0081	0.6932	0.7204	0.0197	0.7019
0.06078	975.	0.4909	0.0057	0.4745	0.4520	0.0129	0.4821
0.03155	101.	0.6876	0.0081	0.6807	0.6808	0.0191	0.6684
0.06206	101.	0.4769	0.0051	0.4764	0.4605	0.0066	0.4574

ENERGY RANGE(EV)=83141.-75223. TOTAL=12.599 CAPTURE=0.2507

AT/BARN	TEFF	TR-OBS	ETR-OB	TR-CAL	SIR-OB	ESR-OB	SIR-CA
0.00758	301.	0.9127	0.0071	0.9092	0.8865	0.0157	0.9098
0.01552	301.	0.8258	0.0064	0.8237	0.8024	0.0142	0.8243
0.03155	301.	0.6823	0.0054	0.6764	0.6690	0.0121	0.6758
0.04670	301.	0.5766	0.0046	0.5632	0.5569	0.0102	0.5605
0.06206	301.	0.4808	0.0039	0.4690	0.4570	0.0086	0.4635
0.02956	975.	0.6947	0.0074	0.6915	0.6914	0.0165	0.6991
0.06078	975.	0.4887	0.0052	0.4722	0.4464	0.0110	0.4780
0.03155	101.	0.6828	0.0074	0.6791	0.6707	0.0167	0.6647
0.06206	101.	0.4797	0.0048	0.4743	0.4563	0.0054	0.4528

ENERGY RANGE(EV)=75223.-68059. TOTAL=12.687 CAPTURE=0.2711

AT/BARN	TEFF	TR-OBS	ETR-OB	TR-CAL	SIR-OB	ESR-OB	SIR-CA
0.00758	301.	0.9118	0.0067	0.9086	0.8843	0.0150	0.9088
0.01552	301.	0.8289	0.0061	0.8226	0.8189	0.0138	0.8225
0.03155	301.	0.6882	0.0051	0.6748	0.6801	0.0117	0.6729
0.04670	301.	0.5765	0.0044	0.5612	0.5620	0.0099	0.5569
0.06206	301.	0.4830	0.0037	0.4669	0.4510	0.0082	0.4597
0.02956	975.	0.7137	0.0069	0.6898	0.7073	0.0158	0.6963
0.06078	975.	0.4897	0.0048	0.4700	0.4568	0.0106	0.4741
0.03155	101.	0.6841	0.0069	0.6776	0.6780	0.0158	0.6608
0.06206	101.	0.4813	0.0045	0.4722	0.4474	0.0048	0.4482

ENERGY RANGE(EV)=68059.-61577. TOTAL=12.773 CAPTURE=0.2927

AT/BARN	TEFF	TR-OBS	ETR-OB	TR-CAL	SIR-OB	ESR-OB	SIR-CA
0.00758	301.	0.9097	0.0066	0.9081	0.8832	0.0143	0.9078
0.01552	301.	0.8264	0.0060	0.8216	0.7759	0.0127	0.8206
0.03155	301.	0.6774	0.0050	0.6732	0.6519	0.0108	0.6700
0.04670	301.	0.5717	0.0043	0.5594	0.5395	0.0092	0.5534
0.06206	301.	0.4781	0.0037	0.4649	0.4564	0.0079	0.4558
0.02956	975.	0.6977	0.0067	0.6882	0.6589	0.0141	0.6937
0.06078	975.	0.4821	0.0047	0.4679	0.4789	0.0107	0.4703
0.03155	101.	0.6785	0.0069	0.6762	0.6433	0.0146	0.6569
0.06206	101.	0.4790	0.0045	0.4702	0.4517	0.0047	0.4435

ENERGY RANGE(EV)=61577.-55712. TOTAL=12.856 CAPTURE=0.3155

AT/BARN	TEFF	TR-OBS	ETR-OB	TR-CAL	SIR-OB	ESR-OB	SIR-CA
0.00758	301.	0.9026	0.0066	0.9075	0.8741	0.0138	0.9068
0.01552	301.	0.8188	0.0060	0.8207	0.8065	0.0126	0.8188
0.03155	301.	0.6706	0.0050	0.6718	0.6652	0.0106	0.6670
0.04670	301.	0.5557	0.0042	0.5577	0.5153	0.0086	0.5498
0.06206	301.	0.4597	0.0036	0.4631	0.4390	0.0074	0.4519
0.02956	975.	0.6940	0.0068	0.6867	0.6841	0.0142	0.6911
0.06078	975.	0.4701	0.0046	0.4660	0.4407	0.0097	0.4666
0.03155	101.	0.6668	0.0072	0.6749	0.6623	0.0152	0.6529
0.06206	101.	0.4593	0.0044	0.4682	0.4301	0.0043	0.4388

ENERGY RANGE(EV)=55712.-50406. TOTAL=12.939 CAPTURE=0.3396

AT/BARN	TEFF	TR-OBS	ETR-OB	TR-CAL	SIR-OB	ESR-OB	SIR-CA
0.00758	301.	0.9085	0.0067	0.9070	0.8723	0.0133	0.9057
0.01552	301.	0.8318	0.0061	0.8197	0.8094	0.0123	0.8169
0.03155	301.	0.6860	0.0051	0.6704	0.6471	0.0101	0.6640
0.04670	301.	0.5662	0.0043	0.5561	0.5471	0.0087	0.5462
0.06206	301.	0.4692	0.0037	0.4613	0.4484	0.0073	0.4479
0.02956	975.	0.7058	0.0069	0.6852	0.6776	0.0137	0.6885
0.06078	975.	0.4801	0.0048	0.4643	0.4634	0.0098	0.4630
0.03155	101.	0.6838	0.0072	0.6736	0.6244	0.0137	0.6489
0.06206	101.	0.4709	0.0046	0.4661	0.4398	0.0040	0.4339

ENERGY RANGE(EV)=50406.-45606. TOTAL=13.021 CAPTURE=0.3649

AT/BARN	TEFF	TR-OBS	ETR-OB	TR-CAL	SIR-OB	ESR-OB	SIR-CA
0.00758	301.	0.8919	0.0067	0.9065	0.9041	0.0133	0.9046
0.01552	301.	0.8182	0.0061	0.8188	0.7959	0.0118	0.8149
0.03155	301.	0.6788	0.0051	0.6690	0.6497	0.0099	0.6609
0.04670	301.	0.5629	0.0044	0.5545	0.5482	0.0085	0.5424
0.06206	301.	0.4692	0.0037	0.4596	0.4359	0.0070	0.4438
0.02956	975.	0.6975	0.0069	0.6838	0.6964	0.0137	0.6860
0.06078	975.	0.4778	0.0048	0.4624	0.4518	0.0094	0.4594
0.03155	101.	0.6709	0.0071	0.6724	0.6499	0.0138	0.6446
0.06206	101.	0.4698	0.0045	0.4639	0.4413	0.0039	0.4290

ENERGY RANGE(EV)=45606.-41262. TOTAL=13.103 CAPTURE=0.3914

AT/BARN	TEFF	TR-OBS	ETR-OB	TR-CAL	SIR-OB	ESR-OB	SIR-CA
0.00758	301.	0.8944	0.0068	0.9060	0.9080	0.0135	0.9034
0.01552	301.	0.8156	0.0062	0.8180	0.8409	0.0125	0.8129
0.03155	301.	0.6666	0.0052	0.6678	0.6658	0.0102	0.6576
0.04670	301.	0.5465	0.0043	0.5531	0.5400	0.0085	0.5386
0.06206	301.	0.4577	0.0037	0.4579	0.4336	0.0070	0.4395
0.02956	975.	0.6931	0.0072	0.6824	0.6747	0.0133	0.6835
0.06078	975.	0.4599	0.0048	0.4607	0.4359	0.0091	0.4558
0.03155	101.	0.6613	0.0072	0.6712	0.6718	0.0145	0.6403
0.06206	101.	0.4674	0.0047	0.4612	0.4279	0.0040	0.4240

ENERGY RANGE(EV)=41262.-37332. TOTAL=13.187 CAPTURE=0.4191

AT/BARN	TEFF	TR-OBS	ETR-OB	TR-CAL	SIR-OB	ESR-OB	SIR-CA
0.00758	301.	0.9018	0.0067	0.9054	0.8767	0.0125	0.9022
0.01552	301.	0.8212	0.0061	0.8171	0.7814	0.0112	0.8107
0.03155	301.	0.6650	0.0051	0.6665	0.6382	0.0094	0.6542
0.04670	301.	0.5551	0.0043	0.5516	0.5303	0.0080	0.5346
0.06206	301.	0.4575	0.0036	0.4562	0.4220	0.0066	0.4351
0.02956	975.	0.6775	0.0068	0.6810	0.6528	0.0127	0.6809
0.06078	975.	0.4605	0.0046	0.4590	0.4285	0.0090	0.4521
0.03155	101.	0.6760	0.0073	0.6701	0.6382	0.0135	0.6359
0.06206	101.	0.4618	0.0044	0.4582	0.4110	0.0037	0.4189

ENERGY RANGE(EV)=37332.-33777. TOTAL=13.272 CAPTURE=0.4479

AT/BARN	TEFF	TR-OBS	ETR-OB	TR-CAL	SIR-OB	ESR-OB	SIR-CA
0.00758	301.	0.8955	0.0067	0.9049	0.8958	0.0127	0.9009
0.01552	301.	0.8096	0.0061	0.8163	0.8057	0.0115	0.8084
0.03155	301.	0.6634	0.0051	0.6653	0.6546	0.0096	0.6507
0.04670	301.	0.5481	0.0043	0.5502	0.5141	0.0078	0.5304
0.06206	301.	0.4594	0.0037	0.4545	0.4255	0.0066	0.4305
0.02956	975.	0.6805	0.0073	0.6796	0.6804	0.0137	0.6783
0.06078	975.	0.4669	0.0050	0.4574	0.4155	0.0089	0.4484
0.03155	101.	0.6628	0.0073	0.6688	0.6395	0.0137	0.6313
0.06206	101.	0.4630	0.0045	0.4545	0.4217	0.0037	0.4138

Table III (continued)

ENERGY RANGE(EV)=33777.-30560. TOTAL=13.359 CAPTURE=0.4778

AT/BARN	TEFF	TR-OBS	ETR-OB	TR-CAL	SIR-OB	ESR-OB	SIR-CA
0.00758	301.	0.8994	0.0068	0.9044	0.8920	0.0128	0.8995
0.01552	301.	0.8181	0.0062	0.8154	0.8123	0.0117	0.8059
0.03155	301.	0.6589	0.0051	0.6641	0.6379	0.0095	0.6470
0.04670	301.	0.5450	0.0043	0.5487	0.5155	0.0079	0.5260
0.06206	301.	0.4481	0.0037	0.4525	0.4160	0.0066	0.4257
0.02956	975.	0.6646	0.0068	0.6783	0.6760	0.0131	0.6756
0.06078	975.	0.4577	0.0048	0.4557	0.4278	0.0089	0.4445
0.03155	101.	0.6595	0.0075	0.6675	0.6378	0.0141	0.6266
0.06206	101.	0.4489	0.0045	0.4498	0.4085	0.0040	0.4088

ENERGY RANGE(EV)=30560.-27649. TOTAL=13.450 CAPTURE=0.5087

AT/BARN	TEFF	TR-OBS	ETR-OB	TR-CAL	SIR-OB	ESR-OB	SIR-CA
0.00758	301.	0.8961	0.0065	0.9039	0.8757	0.0119	0.8979
0.01552	301.	0.8056	0.0059	0.8146	0.7754	0.0107	0.8032
0.03155	301.	0.6507	0.0048	0.6629	0.6267	0.0088	0.6430
0.04670	301.	0.5298	0.0040	0.5471	0.5080	0.0074	0.5214
0.06206	301.	0.4386	0.0034	0.4503	0.4033	0.0061	0.4206
0.02956	975.	0.6672	0.0064	0.6769	0.6617	0.0120	0.6727
0.06078	975.	0.4406	0.0043	0.4541	0.4095	0.0079	0.4405
0.03155	101.	0.6575	0.0072	0.6661	0.6131	0.0134	0.6220
0.06206	101.	0.4372	0.0042	0.4438	0.3910	0.0036	0.4041

ENERGY RANGE(EV)=27649.-25016. TOTAL=13.544 CAPTURE=0.5406

AT/BARN	TEFF	TR-OBS	ETR-OB	TR-CAL	SIR-OB	ESR-OB	SIR-CA
0.00758	301.	0.8858	0.0061	0.9033	0.8904	0.0115	0.8962
0.01552	301.	0.8087	0.0056	0.8197	0.7737	0.0101	0.8003
0.03155	301.	0.6498	0.0045	0.6617	0.6102	0.0083	0.6388
0.04670	301.	0.5438	0.0039	0.5454	0.5004	0.0070	0.5167
0.06206	301.	0.4422	0.0033	0.4477	0.3988	0.0057	0.4154
0.02956	975.	0.6620	0.0061	0.6755	0.6234	0.0109	0.6697
0.06078	975.	0.4440	0.0042	0.4524	0.4068	0.0076	0.4362
0.03155	101.	0.6463	0.0063	0.6644	0.5881	0.0111	0.6174
0.06206	101.	0.4453	0.0041	0.4359	0.3896	0.0034	0.3999

ENERGY RANGE(EV)=25016.-22634. TOTAL=13.643 CAPTURE=0.5734

AT/BARN	TEFF	TR-OBS	ETR-OB	TR-CAL	SIR-OB	ESR-OB	SIR-CA
0.00758	301.	0.8932	0.0061	0.9028	0.9017	0.0116	0.8963
0.01552	301.	0.8077	0.0055	0.8129	0.7900	0.0103	0.7972
0.03155	301.	0.6541	0.0046	0.6604	0.6387	0.0085	0.6345
0.04670	301.	0.5398	0.0038	0.5434	0.5240	0.0072	0.5118
0.06206	301.	0.4483	0.0033	0.4446	0.4172	0.0059	0.4101
0.02956	975.	0.6731	0.0061	0.6742	0.6794	0.0116	0.6666
0.06078	975.	0.4532	0.0042	0.4506	0.4285	0.0079	0.4318
0.03155	101.	0.6590	0.0061	0.6624	0.6392	0.0114	0.6130
0.06206	101.	0.4479	0.0040	0.4257	0.4087	0.0036	0.3967

ENERGY RANGE(EV)=22634.-20478. TOTAL=13.746 CAPTURE=0.6069

AT/BARN	TEFF	TR-OBS	ETR-OB	TR-CAL	SIR-OB	ESR-OB	SIR-CA
0.00758	301.	0.8967	0.0061	0.9022	0.8879	0.0112	0.8922
0.01552	301.	0.8084	0.0056	0.8120	0.7857	0.0099	0.7937
0.03155	301.	0.6507	0.0046	0.6591	0.6053	0.0080	0.6299
0.04670	301.	0.5334	0.0038	0.5411	0.4817	0.0066	0.5069
0.06206	301.	0.4307	0.0032	0.4406	0.3906	0.0055	0.4048
0.02956	975.	0.6660	0.0061	0.6728	0.6358	0.0108	0.6632
0.06078	975.	0.4408	0.0041	0.4488	0.4008	0.0073	0.4271
0.03155	101.	0.6566	0.0063	0.6600	0.6130	0.0112	0.6090
0.06206	101.	0.4360	0.0040	0.4122	0.3917	0.0032	0.3949

ENERGY RANGE(EV)=20478.-18528. TOTAL=13.855 CAPTURE=0.6412

AT/BARN	TEFF	TR-OBS	ETR-OB	TR-CAL	SIR-OB	ESR-OB	SIR-CA
0.00758	301.	0.8986	0.0061	0.9016	0.8831	0.0109	0.8899
0.01552	301.	0.8097	0.0055	0.8111	0.7788	0.0098	0.7900
0.03155	301.	0.6585	0.0045	0.6576	0.6146	0.0080	0.6251
0.04670	301.	0.5441	0.0038	0.5394	0.4941	0.0066	0.5020
0.06206	301.	0.4526	0.0033	0.4355	0.3893	0.0054	0.3998
0.02956	975.	0.6731	0.0060	0.6714	0.6558	0.0109	0.6595
0.06078	975.	0.4571	0.0042	0.4467	0.4023	0.0072	0.4221
0.03155	101.	0.6576	0.0062	0.6568	0.6158	0.0112	0.6059
0.06206	101.	0.4597	0.0041	0.3944	0.3815	0.0028	0.3956

ENERGY RANGE(EV)=18528.-16763. TOTAL=13.970 CAPTURE=0.6761

AT/BARN	TEFF	TR-OBS	ETR-OB	TR-CAL	SIR-OB	ESR-OB	SIR-CA
0.00758	301.	0.8843	0.0060	0.9010	0.8573	0.0106	0.8873
0.01552	301.	0.7921	0.0054	0.8102	0.7442	0.0093	0.7859
0.03155	301.	0.6379	0.0044	0.6549	0.5828	0.0076	0.6203
0.04670	301.	0.5216	0.0037	0.5349	0.4631	0.0062	0.4974
0.06206	301.	0.4281	0.0031	0.4290	0.3646	0.0051	0.3953
0.02956	975.	0.6505	0.0059	0.6699	0.6004	0.0100	0.6555
0.06078	975.	0.4262	0.0039	0.4443	0.3756	0.0068	0.4169
0.03155	101.	0.6394	0.0061	0.6528	0.5767	0.0106	0.6040
0.06206	101.	0.4328	0.0039	0.3710	0.3487	0.0029	0.3998

ENERGY RANGE(EV)=16763.-15167. TOTAL=14.092 CAPTURE=0.7115

AT/BARN	TEFF	TR-OBS	ETR-OB	TR-CAL	SIR-OB	ESR-OB	SIR-CA
0.00758	301.	0.8816	0.0059	0.9004	0.8631	0.0108	0.8843
0.01552	301.	0.7969	0.0053	0.8093	0.7684	0.0097	0.7815
0.03155	301.	0.6383	0.0044	0.6540	0.5872	0.0077	0.6155
0.04670	301.	0.5221	0.0037	0.5305	0.4793	0.0065	0.4934
0.06206	301.	0.4390	0.0031	0.4205	0.3771	0.0053	0.3918
0.02956	975.	0.6552	0.0058	0.6694	0.6343	0.0106	0.6513
0.06078	975.	0.4432	0.0040	0.4416	0.3898	0.0071	0.4116
0.03155	101.	0.6414	0.0061	0.6476	0.5892	0.0109	0.6039
0.06206	101.	0.4434	0.0039	0.3402	0.3779	0.0031	0.4093

ENERGY RANGE(EV)=15167.-13722. TOTAL=14.222 CAPTURE=0.7475

AT/BARN	TEFF	TR-OBS	ETR-OB	TR-CAL	SIR-OB	ESR-OB	SIR-CA
0.00758	301.	0.8902	0.0059	0.8993	0.8733	0.0104	0.8811
0.01552	301.	0.7931	0.0053	0.8083	0.7669	0.0092	0.7768
0.03155	301.	0.6447	0.0044	0.6516	0.6005	0.0075	0.6110
0.04670	301.	0.5361	0.0037	0.5249	0.4694	0.0061	0.4904
0.06206	301.	0.4409	0.0031	0.4093	0.3757	0.0050	0.3900
0.02956	975.	0.6608	0.0058	0.6669	0.6409	0.0103	0.6467
0.06078	975.	0.4349	0.0039	0.4383	0.4011	0.0069	0.4062
0.03155	101.	0.6462	0.0061	0.6407	0.5948	0.0105	0.6068
0.06206	101.	0.4505	0.0039	0.2998	0.3728	0.0032	0.4264

ENERGY RANGE(EV)=13722.-12415. TOTAL=14.359 CAPTURE=0.7839

AT/BARN	TEFF	TR-OBS	ETR-OB	TR-CAL	SIR-OB	ESR-OB	SIR-CA
0.00758	301.	0.8919	0.0058	0.8991	0.8411	0.0096	0.8774
0.01552	301.	0.7984	0.0052	0.8073	0.7257	0.0084	0.7717
0.03155	301.	0.6379	0.0043	0.6488	0.5522	0.0067	0.6071
0.04670	301.	0.5264	0.0036	0.5175	0.4386	0.0055	0.4892
0.06206	301.	0.4339	0.0031	0.3946	0.3561	0.0046	0.3910
0.02956	975.	0.6477	0.0057	0.6652	0.5870	0.0093	0.6418
0.06078	975.	0.4272	0.0038	0.4343	0.3694	0.0063	0.4009
0.03155	101.	0.6401	0.0060	0.6316	0.5492	0.0095	0.6137
0.06206	101.	0.4390	0.0039	0.2470	0.3506	0.0028	0.4545

Table III (continued)

ENERGY RANGE(EV)=12415.-11233.				TOTAL=14.504		CAPTURE=0.8208	
AT/BARN	TEFF	TR-OBS	ETR-OB	TR-CAL	SIR-OB	ESR-OB	SIR-CA
0.00758	301.	0.8879	0.0057	0.8984	0.8629	0.0104	0.8733
0.01552	301.	0.8011	0.0052	0.8062	0.7631	0.0092	0.7663
0.03155	301.	0.6460	0.0043	0.6451	0.5767	0.0073	0.6042
0.04670	301.	0.5327	0.0036	0.5079	0.4625	0.0061	0.4907
0.06206	301.	0.4428	0.0030	0.3753	0.3680	0.0050	0.3962
0.02956	975.	0.6632	0.0057	0.6634	0.6197	0.0101	0.6366
0.06078	975.	0.4427	0.0038	0.4292	0.3882	0.0068	0.3962
0.03155	101.	0.6501	0.0060	0.6197	0.5718	0.0104	0.6266
0.06206	101.	0.4510	0.0038	0.1781	0.3626	0.0032	0.4983

ENERGY RANGE(EV)=11233.-10163.				TOTAL=14.659		CAPTURE=0.8582	
AT/BARN	TEFF	TR-OBS	ETR-OB	TR-CAL	SIR-OB	ESR-OB	SIR-CA
0.00758	301.	0.8903	0.0057	0.8977	0.8678	0.0100	0.8686
0.01552	301.	0.7986	0.0051	0.8050	0.7491	0.0087	0.7607
0.03155	301.	0.6508	0.0043	0.6405	0.5791	0.0070	0.6031
0.04670	301.	0.5318	0.0036	0.4953	0.4467	0.0057	0.4962
0.06206	301.	0.4437	0.0030	0.3499	0.3647	0.0048	0.4075
0.02956	975.	0.6583	0.0056	0.6615	0.6184	0.0097	0.6313
0.06078	975.	0.4429	0.0038	0.4228	0.3760	0.0064	0.3924
0.03155	101.	0.6501	0.0060	0.6039	0.5729	0.0101	0.6478
0.06206	101.	0.4487	0.0038	0.0883	0.3635	0.0030	0.5639

(a) Reading Guide of Table III

1) ENERGY RANGE (EV) = Energy interval, ΔE, over which the transmission and the self-indication are averaged in units of eV.

2) TOTAL = Average total cross section, $\langle \sigma_t \rangle$, (s- and p-wave included) in units of barns.

3) CAPTURE = Average radiative capture cross section (s- and p-wave included) in units of barns.

4) AT/BARN = Shielding sample thickness, n, measured in units of atom/barn.

5) TEFF = Effective temperature (^{o}K).

6) TR-OBS = Average transmission observed.

7) ETR-OB = Observed standard error of experimental average transmission.

8) TR-CAL = Calculated average transmission by analytical method.

9) SIR-OB = Observed self-indication ratio.

10) ESR-OB = Observed standard error of the self-indication ratio.

11) SIR-CA = Calculated self-indication ratio by analytical method.

TABLE IV

The Best Fit Average Resonance Parameters Obtained by Analytical Calculation.

	S-Wave $J = \frac{1}{2}$	P-Wave	
		$J = \frac{1}{2}$	$J = 3/2$
Strength Function	0.93×10^{-4}	2.3×10^{-4}	2.3×10^{-4}
Level Space	19.5 eV	19.5 eV	9.75 eV
Reduced Width	0.00181 eV	0.00487 eV	0.00243 eV
Radiation Width	0.0230 eV	0.0230 eV	0.0230 eV
Nuclear Radius	$R=0.90 \times 10^{-12}$ cm		

TABLE V

The Goodness of Fit Obtained by Average Resonance Parameters on Table IV for each Sample and Temperature.

Sample Thickness (atom/barn)	effective temp. (^{o}K)	ΔR[(a)] Averaged over energy range 91.5 to 12.4 keV	
		Average Transmission	Self-indication Ratio
0.00758	301	1.27	1.47
0.01552	301	1.18	1.81
0.03155	301	1.70	1.98
0.04670	301	2.02	2.20
0.06206	301	3.26	2.09
0.02956	975	1.60	1.61
0.06078	975	2.07	2.55
0.03155	101	1.02	1.41
0.06206	101	5.01	5.63
$\langle \Delta R \rangle$[(b)]	2.22		

*(a) $$\overline{\Delta R} = \sum_{i}^{N} \left\{ \frac{\left| R^{exp} - R^{cal} \right|}{\Delta R^{exp}} \right\}_i \Big/ N$$

(b) $\langle \Delta R \rangle \equiv$ ΔR averaged over all sets of data point

NEUTRON TOTAL CROSS-SECTION MEASUREMENTS ON ^{54}FE, ^{61}NI AND ^{64}NI

R. W. Hockenbury, N. N. Kaushal and R. C. Block

Transmission measurements were made on ^{54}Fe, ^{61}Ni and ^{64}Ni using a ^{10}B-NaI detector at 28 meters. The LINAC was run with a 20 nsec pulse width at 500 pps with a minimum channel width of 31.25 nsec. The samples were cycled under computer control to average out linac intensity fluctuations. These transmission data will be combined with capture data[1] to obtain resonance parameters for these isotopes.

For this resolution and sample thickness, the useful energy range extends up to several tens of keV. The samples will later be repacked for higher resolution experiments up to several hundred keV.

REFERENCE:

1. See this report, p. 38.

NEUTRON CAPTURE MEASUREMENTS ON ^{54}FE

B. J. Ward,* R. W. Hockenbury, N. N. Kaushal
and R. C. Block

The ^{54}Fe (48.7 grams sample) capture yield has been obtained from 5 to 200 keV. Pulse-height vs. time-of-flight data were taken in order to obtain the capture detector efficiency for the yield calculation. The neutron flux was measured using a ^{10}B-NaI detector, with the absolute flux normalized to the 1.15 keV ^{54}Fe resonance area observed in an Fe foil. This Fe foil had been previously cross-calibrated to an Au foil.

Nine new resonances were observed for ^{54}Fe and the resonance capture areas ($\sigma_o\Gamma_\gamma$) have been obtained. The 11.2 keV resonance previously attributed to ^{56}Fe has been found to be due to ^{54}Fe. A resonance near 22.9 keV has been shown to exist in both ^{54}Fe and ^{56}Fe.

*Based in part on the Master's Engineering Project of B. J. Ward.

ANALYSIS OF NEUTRON CAPTURE DATA FOR ^{54}FE, ^{58}FE, ^{61}NI AND ^{64}NI

R. W. Hockenbury, N. N. Kaushal and R. C. Block

The time-of-flight neutron spectrum has been measured and converted to relative neutron flux. This flux will be used to obtain capture yields for ^{54}Fe, ^{58}Fe, ^{61}Ni and ^{64}Ni.

Isotopic assignments have been made for these isotopes up to the tens of keV region with the aid of our previous capture results.[1,2] (See Tables 1 through 4) Several discrepancies were noted in previous assignments which were due to the previous lack of a ^{54}Fe sample and also poorer resolution. When the present measurements are extended to 200 keV with better resolution, isotopic assignments will be continued to higher energies than shown in the Tables. We note that without a ^{62}Ni sample, some uncertainties are caused in the present assignments.

The next step in the analysis wil be to determine resonance parameters, using both capture and transmission[3] data.

REFERENCES:

1. R. W. Hockenbury, et al., Phys. Rev., 178, 1746 (1969).
2. R. G. Stieglitz et al., Nucl. Phys., A163, 592 (1970).
3. See this report, p. 36.

Table 1

^{54}Fe

E_o (keV)	E_o (keV)
3.10	23.0
8.10	28.2
9.48	30.6
11.2	35.1
13.5	38.3
14.4	39.1
19.2	

Table 2

^{58}Fe

E_o (keV)
0.230
0.359
6.20
10.5
19.2

Table 3

^{61}Ni

E_o (keV)	E_o (keV)
1.35	11.4
2.35	11.8
3.14	12.6
3.30	13.3
3.39*	13.5
4.59*	13.9
6.36	14.3
6.46	15.3
7.11	16.7
7.52	17.7
8.70	18.8
9.87	20.0
10.1	20.4
10.9	21.3

*Assignment not definite - probably ^{61}Ni

Table 4

^{64}Ni

E_o (keV)
14.3
25.8
31.8
32-35*
39.2 *
45.8 *
60.0 *
62.4
82.8

*Unresolved

NEUTRON CAPTURE AND FISSION CROSS SECTIONS OF ^{242}PU

R. W. Hockenbury and R. C. Block

Preliminary absorption experiments have been performed on ^{242}Pu using the 1.25-meter liquid scintillator. Since another experiment was controlling the LINAC, the ^{242}Pu measurements were done as a satellite experiment using a small time-of-flight analyzer and the existing LINAC operating parameters (pulse width of 250 nsec at a 330 pps repetition rate).

The detector was operated in a high-low bias mode to separate capture and fission events. Five overlapping runs were made, covering the range from 60 eV to 90 keV.

The purpose of the runs was to investigate the foreground-to-background counting rates in the resonance and keV region. Approximately 35 resonances were seen in the range from 60 eV to 1 keV. More resonance structure was observed but not resolved up to about 3 keV. The high-bias data (mostly fission) show prominent clusters of resonances at about 560 and 750 eV even for a short run (about 1½ hours). They represent subthreshold fission in the ^{242}Pu.

The resonance data have been compared to previous total cross section data[1,2] and also to fission data.[3,4] The foreground-to-background ratio has been obtained in the keV region for capture measurements on ^{242}Pu. Suitable LINAC operating conditions can now be selected on the basis of these preliminary runs.

The ^{242}Pu sample (7.7 grams) is fairly radioactive, thus requiring off-line tests for gain shifts and counting rate effects.

REFERENCES:

1. N. J. Pattenden, International Conference on the Study of Nuclear Structure with Neutrons, Antwerp, P93 (1965).
2. T. E. Young and S. D. Reeder, Nucl. Sci. Eng., 40, 389 (1970).
3. D. W. Bergen and R. R. Fullwood, Nucl. Phys., A163, 577 (1971).
4. G. F. Auchampaugh, J. A. Farrell and D. W. Bergen, Nucl. Phys., A171, 31 (1971).

EFFECT OF BREMSSTRAHLUNG END POINT ON THE NEUTRON SPECTRUM FROM THE RPI "BOUNCE" TARGET

R. Zuhr,* Z. Bell and K. Min

We have previously reported the results of angular distribution studies for neutrons scattered from natural iron. These cross sections were measured relative to a lead standard, and thus include the error inherent in the data for that standard. In order to eliminate this source of error, the absolute measurement of differential cross sections is being investigated.

The first step in this investigation was to study the consistency of the neutron energy spectrum as a function of end point energy of the RPI LINAC. Runs were made at 50 and 60 MeV, and the ratio of the number of counts at 60, to that at 50, is given in Fig. 1. Each point represents an average over 20, 32 nsec time-of-flight channels. The graph covers energies from the gamma flash (the high channels at the left) to below 1 keV. The lines are drawn at plus or minus one standard deviation. It should be noted that the ratio is not normalized to unity, but should merely be consistent throughout. The results do fall within the indicated standard deviations and thus provide a basis for further work on absolute measurements.

FIGURE CAPTION

Fig. 1 Ratio of Neutron Energy Spectra for End Point Energies of 60 and 50 MeV.

*Based in part on the Ph.D. Thesis of R. Zuhr.

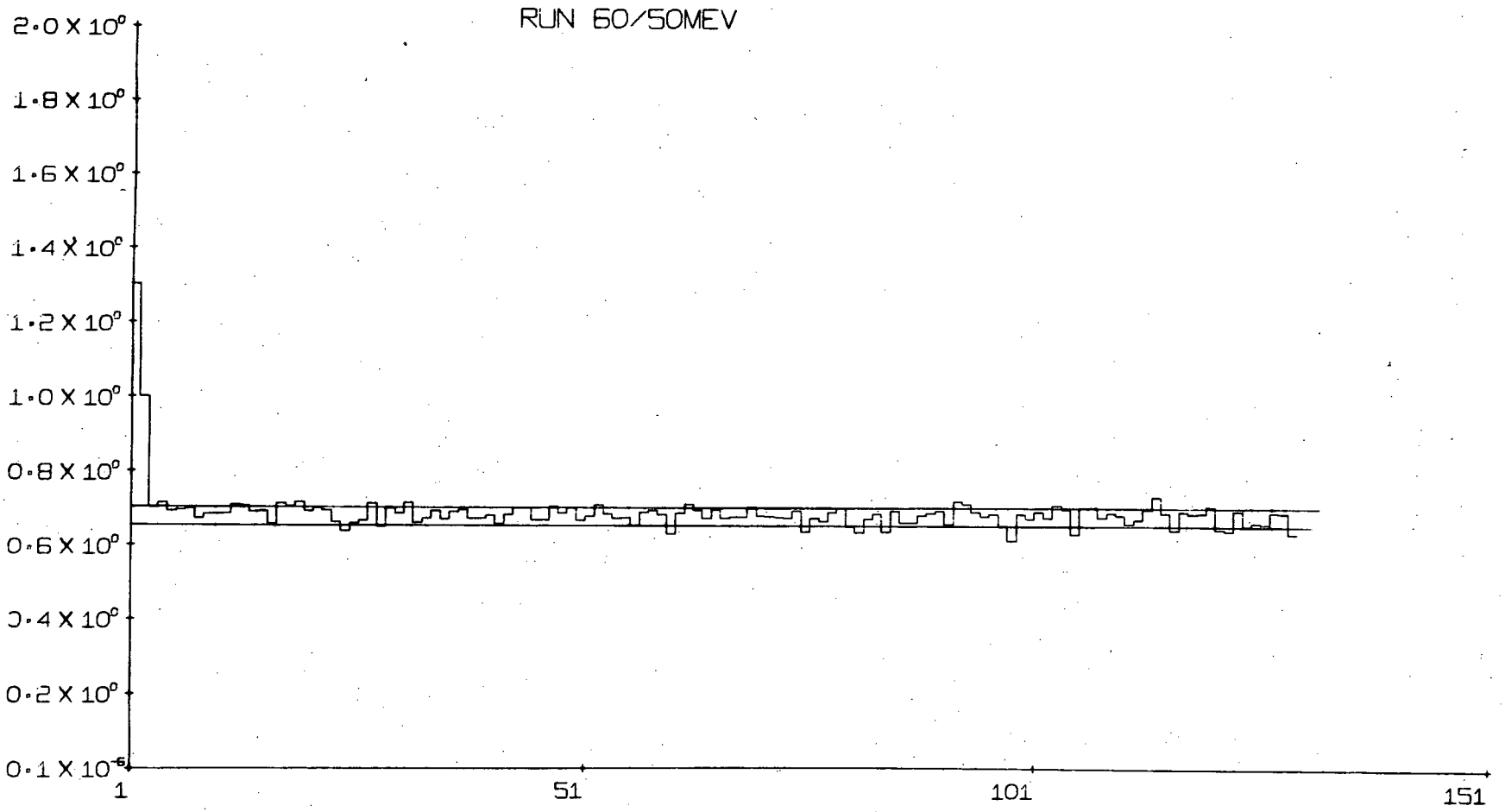
RUN 60/50MEV
2·0 X 10⁰
1·8 X 10⁰
1·6 X 10⁰
1·4 X 10⁰
1·2 X 10⁰
1·0 X 10⁰
0·8 X 10⁰
0·6 X 10⁰
0·4 X 10⁰
0·2 X 10⁰
0·1 X 10⁻⁶
1
51
101
151

Figure 1

R-MATRIX FIT TO IRON TOTAL CROSS-SECTION MINIMA

K. Alfieri* and P. J. Turinsky

Employing the previously reported calculated experimental resolution function[1] for our natural iron thick sample transmission experiment,[2] we have performed an R-Matrix shape analysis to the transmission spectra ratio (TSR); that is, resonance parameters have been adjusted such that agreement between experimental and calculated TSR in the energy regions of deep total cross-section minima have been obtained.

A reduced R-Matrix formalism containing multi-level effects has been employed to parameterize the total cross section, where only S-wave scattering is considered. Since thick sample transmission experiments render no information on peak cross-section behavior, we first calculated the TSR (14" over 20" sample) employing the Columbia resonance parameter set[3] for natural iron. Comparing calculated and experimental TSR in the energy regions of cross-section minima from 20 to 190 KeV, we surmise that the Columbia resonance parameter set is inadequate for predicting minima. Figure 1 illustrates the representative agreement between calculated (Columbia resonance parameters) and experimental TSR. Best agreement was obtained with the Columbia results for the 24 KeV minima, as depicted in Fig. 2. By adjusting the reduced neutron widths of the two resonances bracketing the 24 KeV minima, the improved agreement between experimental and calculated TSR as also shown in Fig. 2 was obtained. Figure 3 indicates the corresponding total cross section obtained by the adjusted resonance parameter set. Excellent agreement with ENDF/B-III (MAT 1180) is obtained for the 24 KeV minima, but disagreement with the cross sections constructed from the Columbia resonance parameter set and more recent Columbia thick sample experiments[4] is obvious. We have not been able to deduce adjusted resonance parameters for the higher energy cross-section minima of natural iron due to poor experimental resolution.

---

*Based in part on the Master's Engineering Project of K. Alfieri.

On reexamination of our previously published Table of transmission area ratios,[5] an error was detected in calculating the error bounds on the % error. Table 1 presents the corrected results, which indicate that our previous conclusions are essentially unaltered. Also indicated in Table 1 are the RPI area ratios (14" over 20" sample and referred to as R in Ref. 5) where small values indicate deep effective iron cross-section minima. This serves as a guide to ranking relative importance of a given minima. Comparing ENDF/B-III (MAT 1180) and ØRNL (MAT 1124), it was determined that only the 24 KeV total cross-section minima was adjusted, with all other minima identical. Hence, our conclusion regarding the inadequacy of ØRNL (MAT 1124) also applies to ENDF/B-III (MAT 1180) with regard to predicting minima in the natural iron total cross section from 70 to 1400 KeV.

REFERENCES:

1. Linear Accelerator Project Progress Report, October - December 1971, 46, COO-3058-11.
2. Linear Accelerator Project Progress Report, October - December 1971, 2, COO-3058-11.
3. J. Garg, J. Rainwater and W. W. Havens, Phys. Rev., 3C, 2447 (1971).
4. F. Rahn et al., Nucl. Sci. Eng., 47, 372 (1972).
5. Linear Accelerator Project Progress Report, October - December 1971, 7, COO-3058-11.

FIGURE CAPTIONS

Fig. 1 Comparison of TSR for Natural Iron from Experiment and Calculated Values Using Columbia Resonance Parameters for 118 to 129 KeV Region.

Fig. 2 Comparison of TSR for Natural Iron from Experiment and Calculated Values Using Columbia and Adjusted Resonance Parameters for 23 to 25 KeV Region.

Fig. 3 Total Cross Section of Natural Iron in Neighborhood of 24 KeV Minima.

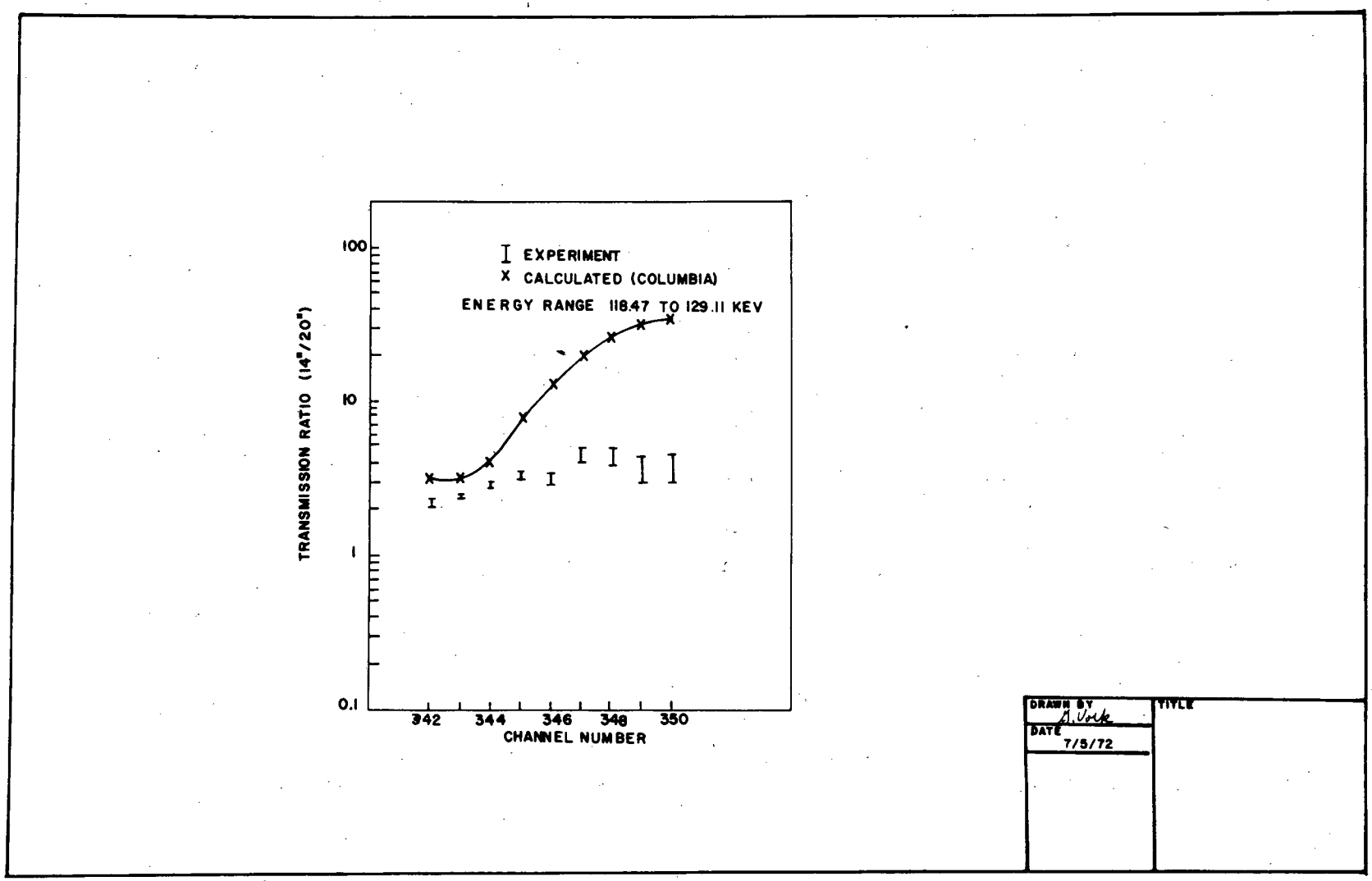
EXPERIMENT
CALCULATED (COLUMBIA)
ENERGY RANGE 118.47 TO 129.11 KEV
TRANSMISSION RATIO (14°/20°)
100
10
1
0.1
342
344
346
348
350
CHANNEL NUMBER
DRAWN BY
A. Vork
DATE
7/5/72
TITLE

Figure 1

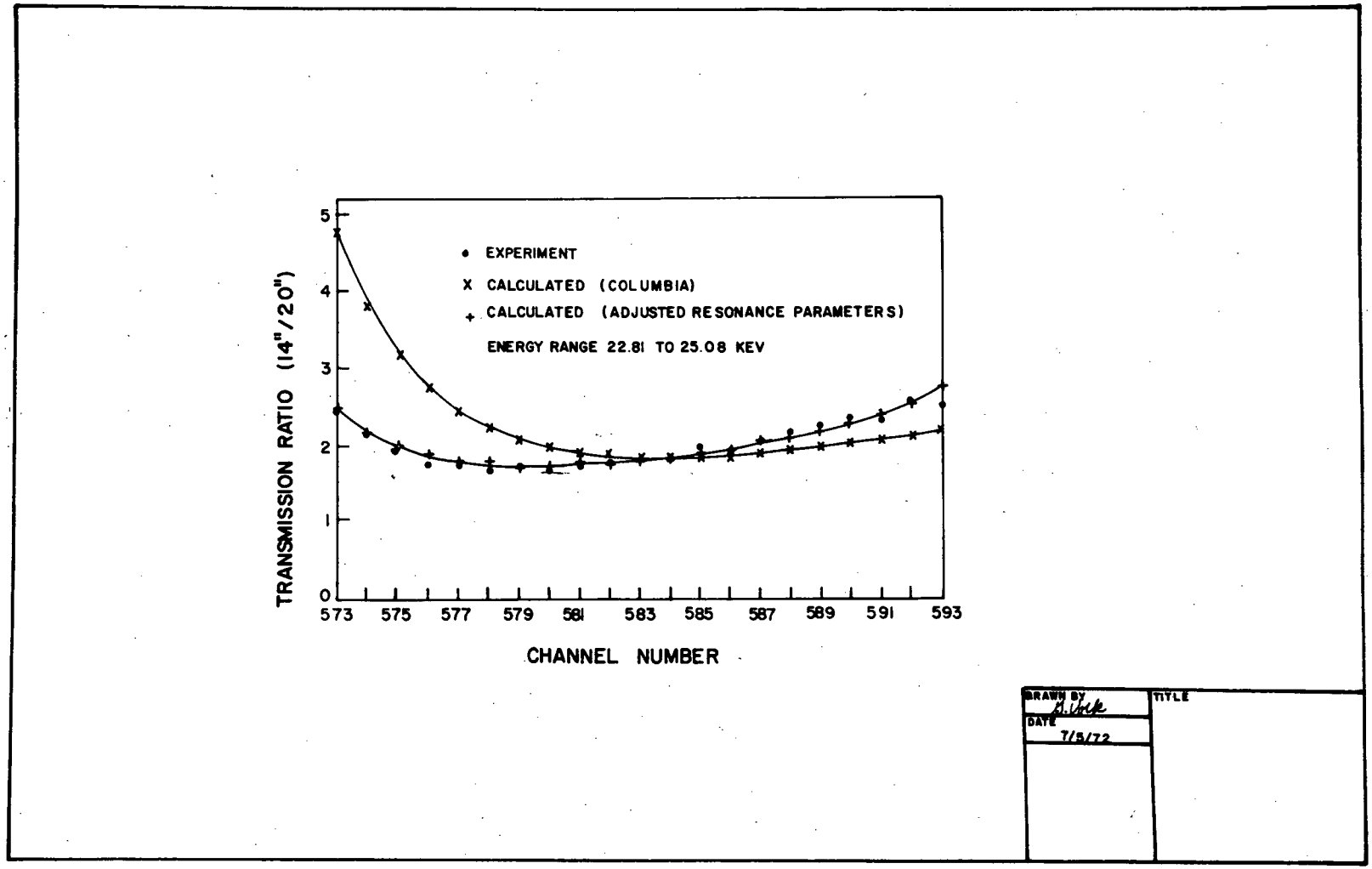
TRANSMISSION RATIO (14"/20")
CHANNEL NUMBER
EXPERIMENT
CALCULATED (COLUMBIA)
CALCULATED (ADJUSTED RESONANCE PARAMETERS)
ENERGY RANGE 22.81 TO 25.08 KEV
0
1
2
3
4
5
573
575
577
579
581
583
585
587
589
591
593
DRAWN BY
DATE
7/5/72
TITLE

Figure 2

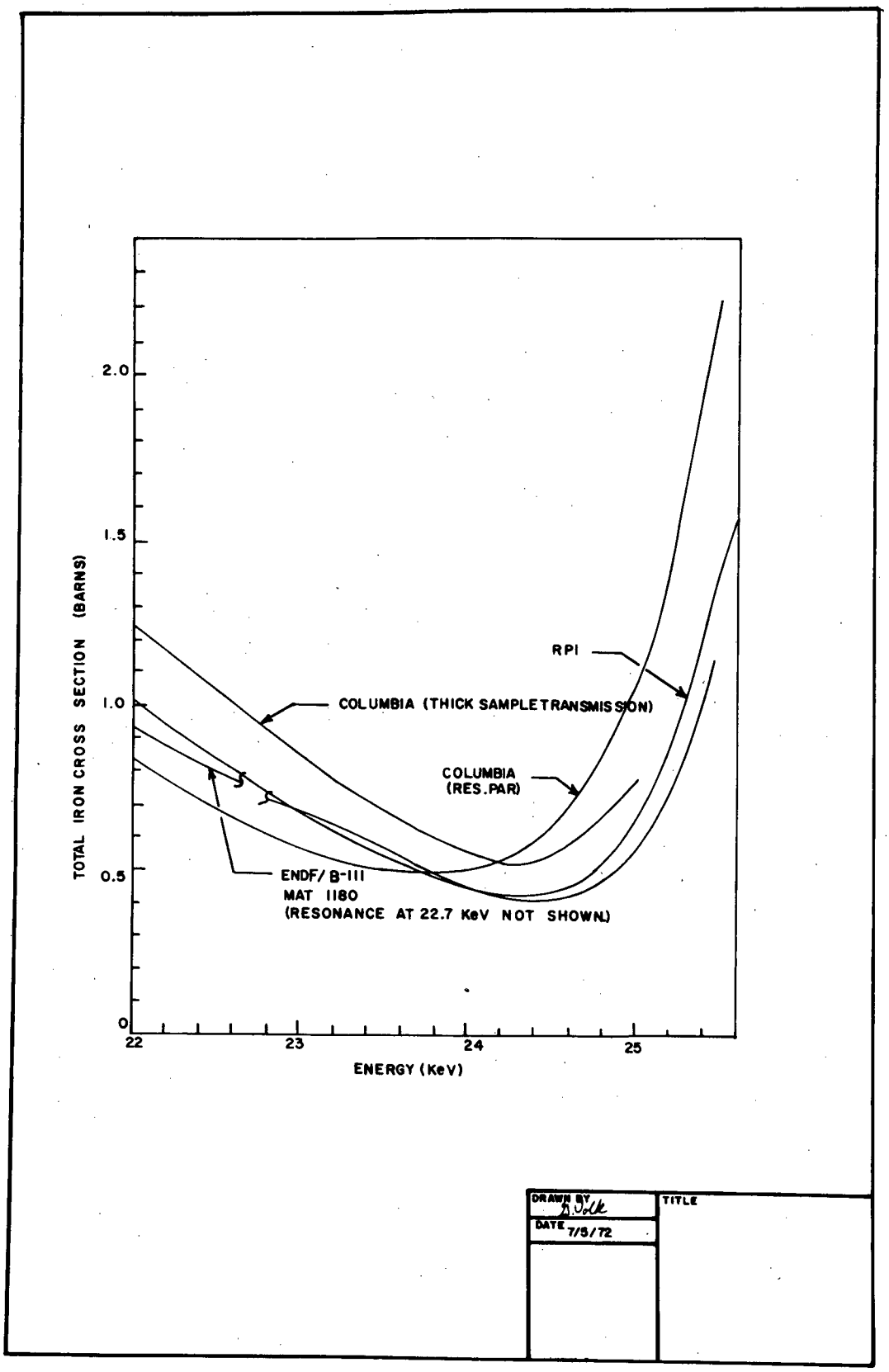
TOTAL IRON CROSS SECTION (BARNS)
2.0
1.5
1.0
0.5
0
22
23
24
25
ENERGY (KeV)
RPI
COLUMBIA (THICK SAMPLE TRANSMISSION)
COLUMBIA
(RES. PAR)
ENDF/B-III
MAT 1180
(RESONANCE AT 22.7 KeV NOT SHOWN)
DRAWN BY
DATE 7/5/72
TITLE

Figure 3

Table 1

Comparison of Experimental and Total Iron Cross Sections from Files ØRNL 1124 and Version 19 through Minima by Area Analysis

Energy Range (KeV)	Area Ratio (14"/20")	ØRNL 1124 Relative Error (ε)	ØRNL 1124 Comparison with RPI's Cross Sections	VERSION 19 Relative Error (ε)	VERSION 19 Comparison with RPI's Cross Sections
20.2 - 27.0	2.1	13 ± 1%	Under	- 6 ± 1%	Over
76.8 - 83.0	2.1	-204 ± 1%	Over	-18 ± 1%	Over
114.8 - 130.5	2.7	-148 ± 2%	Over	-16 ± 2%	Over
132.0 - 139.6	1.8	- 57 ± 1%	Over	-44 ± 1%	Over
155.2 - 169.2	2.0	-133 ± 2%	Over	-19 ± 2%	Over
171.3 - 187.6	2.8	26 ± 2%	Under	-13 ± 2%	Over
203.4 - 224.6	2.2	-202 ± 2%	Over	-19 ± 2%	Over
231.2 - 278.1	2.4	-112 ± 2%	Over	- 8 ± 2%	Over
282.7 - 317.8	2.3	-103 ± 1%	Over	21 ± 1%	Under
323.3 - 387.9	2.3	- 7 ± 1%	Over	4 ± 1%	-
419.2 - 505.2	2.6	- 33 ± 3%	Over	-	-
527.9 - 740.2	3.1	- 4 ± 2%	-	-	-
802.3 - 1413.2	4.6	- 6 ± 4%	-	-	-

STRENGTH FUNCTION CALCULATIONS VIA SPHERICAL OPTICAL MODEL-I

J. Sierra* and P. J. Turinsky

As reported previously,[1] the optical model code JUPITØR has been employed to calculate s-wave strength functions (S_o), p-wave strength functions (S_1) and potential scattering lengths (R′) from mass 20 through 240. This work was undertaken to obtain global optical model parameters to fit all three physical quantities simultaneously, in particular the deep S_1 minima at mass 55 and 160. Our conclusion was that such a simultaneous fit was not likely with the standard spherical optical model potential (SOMP). We have undertaken work to determine whether a modified SOMP, with possible angular momentum dependence other than spin-orbit, would prove more successful.

Noting the implicit complexity of the JUPITØR code due to coupled-channel capability, we have chosen to employ the spherical optical model code ABACUS-II for our continuing studies. We have found ABACUS easily modifiable in contrast to JUPITØR. Our initial work has been to modify ABACUS so as to render agreement with JUPITØR for strength function calculations. As reported by Kikuchi,[2] the proportionality constant used in the ABACUS calculation of the neutron wave number was changed for consistency with JUPITØR, this causing approximately up to 6% changes in S_o, 4% changes in S_1 and 1% changes in R′ for the RPI optical parameters.[1] On automated mass number (A) scans we found that the internal-external wave function matching radius value was not recalculated for each A as desired, hence the code was altered. With these modifications of ABACUS, S_o, S_1 and R′ predictions were in agreement with JUPITØR results. Having established the consistency of the ABACUS and JUPITØR codes, work is now progressing on developing a modified SOMP from a joint ad-hoc-theoretical basis allowing simultaneous fits to S_o, S_1 and R′.

REFERENCES:

1. Linear Accelerator Project Annual Technical Report, October 1, 1970 - September 30, 1971, 149, COO-3058-1.

2. Y. Kikuchi, CEA-N-1532(E), Centre d'Etudes Nucleaires de Saclay (1972).

*Based in part on the Master of Science work of J. Sierra.

DEPARTURES FROM STATISTICAL CROSS-SECTION BEHAVIOR

P. J. Turinsky

Total neutron cross-section measurement on ^{60}Ni [1] about 0.5 MeV performed at RPI indicate an anomalous broad resonance with fine structure. Similar observations on energy averaged cross sections have been noted for ^{40}Ca [2] and other nuclei. A common explanation for such structure is that of intermediate structure, usually doorway states. If indeed this interpretation was correct, reduced reaction widths would no longer satisfy simple distributions (example: Porter-Thomas for reduced neutron widths). Hence the validity of extrapolating reduced widths from the resolved to unresolved region and employment of Monte Carlo (Ladder) or integral approaches to unresolved resonance region group cross sections generation would be dubious. Since within standard statistical distributions, such as Porter-Thomas or Wigner, not likely events still occur, it was considered desirable to quantify what the chances are that an anomalous broad cross-section resonance is produced from normal width and level spacing distribution laws.

Following the work of Baglan, et al.,[3] a computer code has been written which statistically generates the total neutron cross section and analyzes its statistical behavior. That is, supplying as input average reduced widths and level spacing along with other target nucleus properties, distribution functions for these average parameters are employed in Monte Carlo calculations to generate the total cross section for a specified energy range. Samplings from the distributions are only accepted if these averages agree within limits with the specified averages given as input. A reduced R-Matrix formalism allowing multi-level effects is employed for the cross-section reconstruction. Energy averaged cross sections are then calculated for various specified averaging intervals. Having repeated this calculation many times, set averages of the energy averaged cross sections are computed.

From the statistically generated sets of energy averaged cross sections, tests are made to determine how frequently deviations in magnitude from the set averages occur. For example, suppose we are interested in deviations in energy averaged cross sections greater than two times the set averages. Frequency of such deviation occurrences as cataloged by structure width and contributing levels is then computed for each energy averaging interval. From calculated frequency, predictions of how often in energy a given class of anomolous structure would be expected to be observed are computed.

Hence, having performed a cross-section measurement where anomolous structure is observed, the above procedures can be employed to quantify how likely this observation is within the framework of normal distributions. If the observation is highly unlikely, an indication of intermediate structure is suggested invalidating the employment of normal distribution functions. The computer code that performs the statistical analysis has been written and is nearing confirmed operational status. Applications to analyze ^{60}Ni and $^{-40}$Ca total neutron cross sections for possible intermediate structure will be undertaken and reported on in the future.

REFERENCES:

1. P. Stoler, et al., Proc. Third Conf. Neutron Cross Sections and Technology, CONF.-710301, Vol. 1, 311 (1971).
2. G. J. Kirouac, private communication (1972).
3. R. J. Baglan, C. D. Bowman and B. L. Berman, Phys. Rev., C3, 2475 (1971).

REACTOR PHYSICS AND ENGINEERING - EXPERIMENTAL

NEUTRON EMISSION-TIME EFFECTS IN A PULSED SODIUM ASSEMBLY

N. N. Kaushal, B. K. Malaviya, A. N. Mallen
and E. R. Gaerttner

The following summary of a paper has been submitted for presentation at the Winter 1972 Meeting of the American Nuclear Society at Washington, D. C.

SUMMARY

A knowledge of the emission-time effects is important for a correct interpretation of the neutron spectra measured by time-of-flight techniques[1] for two reasons. Firstly, the first time moment or the mean emission time is included in the time of flight and hence must be subtracted to obtain the correct neutron energy. Secondly, the higher time moments have the effect of "time smearing" resulting in a deterioration of the energy resolution of the system. This effect should be taken account of in interpreting sharply structured spectra.

In the course of our experiments on fast neutron transport in a sodium assembly, a simple experiment was performed to obtain information on both counts.[2] Neutron spectrum from the Ta-Pb target was filtered through a 10-inch thick iron stack (placed in the neutron path 10 meters away from the source) and the filtered spectrum recorded by time of flight. The same neutron target was then embedded in the sodium assembly. The neutron spectrum from the sodium assembly ($r \cong 14"$, $\theta \cong 135^{o}$), filtered through the same iron filter was then recorded by means of the same time-of-flight system.

The two time-of-flight spectra are shown in Fig. 1. A comparison of the two spectra shows up some interesting features. The gamma flash which occurred around channel 161 showed up in essentially one time channel in both spectra, thus verifying that the resolution and timing of the system were identical in the two cases. Features corresponding to structure in the neutron spec-

trum, however, are both broadened and shifted to higher times in the spectrum from the assembly. The shift and broadening get progressively larger with decreasing neutron energies. Table 1 lists the time-shifts which should correspond to mean emission time, as a function of neutron energy. Only a small fraction of these shifts can be attributed to a simple (one collision) difference in flight path length in the two cases.

Information on the resolution broadening effect as a function of neutron energy can also be obtained from these data by "smearing" the bare-target spectrum with an energy-dependent resolution function to obtain a "best fit" with the spectrum from the assembly.

We have performed calculations of these time moments using DTF IV code and ENDF/B-II data. While there is qualitative agreement, there are large quantitative discrepancies in the calculated and experimental values.

REFERENCES:

1. B. K. Malaviya, N. N. Kaushal, M. Becker, E. T. Burns, A. Ginsberg and E. R. Gaerttner, Nucl. Sci. Eng., 47, 329 (1972).

2. N. N. Kaushal, B. K. Malaviya, J. F. Lewis, A. N. Mallen and E. R. Gaerttner, "Measurement of Neutron Spectra in a Sodium Assembly," Linear Accelerator Project Annual Technical Report, COO-3058-1, Rensselaer Polytechnic Institute.

FIGURE CAPTION

Fig. 1 Comparison of Neutron Spectra Filtered through a 10-inch Iron Filter from (a) Bare Neutron Target, (b) with Target Embedded in the Sodium Assembly and the Neutron Spectrum from $r \cong 14"$ and $\theta \cong 135^{o}$.

TIME-OF-FLIGHT NEUTRON SPECTRUM
THRU 10 INCH IRON FILTER

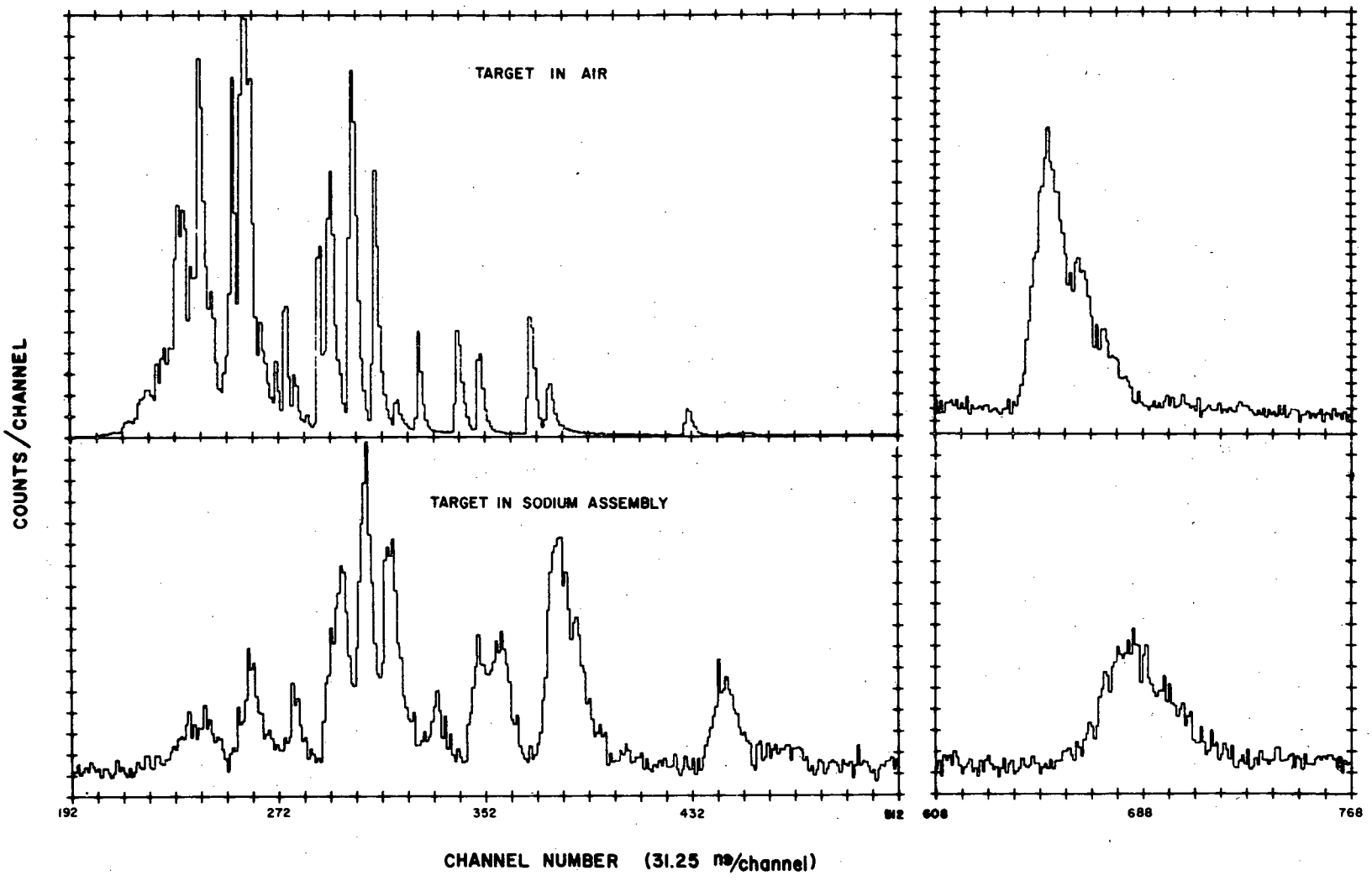

Figure 1

Table 1

Neutron Emission Times in a Sodium Assembly

Energy keV	Channel No. Target in Air	Channel No. Target in Sodium	Δ(Ch)	Emission Time
650	256	260	4	125
350	292	296	4	125
310	300	306	6	187
270	309	315	6	187
220	326	333	7	218
180	341	349	8	250
165	350	358	8	250
130	373	382	9	281
80	430	442	12	375
25	651	684	33	1031

TARGET DEVELOPMENT PROGRAM

A. N. Mallen,* N. N. Kaushal, B. K. Malaviya
and E. R. Gaerttner

During the last quarter, the Fast Spectra air-cooled target insert[1] was disassembled after four years of use. It was observed that approximately 20% of the coolant channel area was blocked by carbon deposits from oil in the cooling air. No other signs of damage were observed in the target, indicating that air-cooling was adequate for the 500 watts of operating power.

A new target and target insert are being constructed to provide positive, leakproof oil cooling to both the target and target insert. The new target is a hollow stainless steel sphere that is filled with lead shot and will be cooled by forced oil convection. Initial tests of power capabilities of the new target and target insert will be performed in the next quarter.

The new target is designed for use with the sodium assembly and is expected to yield improved signal-to-background ratios for all energies but especially below 10 Kev.

REFERENCE:

1. E. Greenspan, B. K. Malaviya and E. R. Gaerttner, "Neutron Target Development Program," Linear Accelerator Project Progress Report, RPI-328-97, 49-63 (1967).

---

*Based in part on the Ph.D. Thesis of A. N. Mallen.

FAST NEUTRON SPECTRA IN A SODIUM ASSEMBLY

N. N. Kaushal, B. K. Malaviya, A. N. Mallen
and E. R. Gaerttner

Measurements of fast neutron spectra in our sodium assembly are continuing.[1] Spectra have been measured at several points in the assembly. These data are now being processed and special attention is being given to the overlap region in the data from the two different detectors used to separately cover the high and the low energy parts of the neutron spectrum. In this connection, the electronics associated with the proton-recoil detector have been modified to obtain better stability and a procedure has been developed to perform quantitative checks on the stability of the detector efficiency. These changes and procedural developments will be described in the next Progress Report.

REFERENCE;

1. Linear Accelerator Project Annual Technical Report, October 1, 1970 - September 30, 1971, COO-3058-1, Rensselaer Polytechnic Institute.

MEASUREMENT OF TIME-DEPENDENT SLOWING-DOWN SPECTRA IN LEAD

N. N. Kaushal

A few preliminary measurements of time-dependent fast neutron spectra in a lead assembly* were carried out using the ^{3}He Solid State sandwich detector.[1] There are two main objectives to these measurements. Firstly, it is to understand the neutron slowing down mechanism and its sensitivity to the elastic and inelastic cross sections in lead; and secondly, it is to understand the behavior of the lead pile as a neutron slowing down spectrometer.[2]

Preliminary experiments were carried out at 20 watts electron beam power. The γ-flash problem was essentially non-existent, and the neutron flux was adequate to provide meaningful data in a few hours. Problems were encountered with excessive RF noise pick-up. Efforts are being made to eliminate this problem.

The data indicate that there is a sharp increase in neutron decay-rate for neutron energies above approximately 500 keV. This could be attributed to increased slowing-down due to inelastic scattering which is significant at these energies.

The experiment will be repeated to check the accuracy of these observations.

REFERENCES:

1. Linear Accelerator Project Annual Technical Report, October 1, 1968 - September 30, 1969, 103, RPI-328-171.
2. L. E. Lazareva, E. L. Feinberg and F. L. Shapiro, Trans. Soviet Physics JETP 2, 351 (1956).

*The use of the lead assembly was made available through the courtesy of R. E. Slovacek et al., Knolls Atomic Power Laboratory.

REACTOR PHYSICS AND ENGINEERING - THEORETICAL

REACTOR THEORY AND ANALYSIS

M. Becker, M. Danchak,[#] G. Epstein,[*] A. Ginsberg[*]
and S. Kang[*]

As a first step in improving the speed with which multigroup constants can be generated, the following procedure has been incorporated into SUPERTOG. The slowing down density for the kth moment at the bottom of a group is given by

$$q_k(u_g) = \left[\sum_{k'} \xi_{kk'} \Sigma^c_{k'}(u_g) \right] \phi_k(u_g) \tag{1}$$

where the c superscript denotes center of mass and the $\xi_{kk'}$ is an integral

$$\xi_{kk'} = \frac{2k'+1}{2} \int_{-1}^{1} P_k[\mu_o(\mu_c)] \, U(\mu_c) \, P_{k'}(\mu_c) d\mu_c \tag{2}$$

These equations are discussed in some detail by Amster.[1] Quantities U, μ_o, μ_c represent respectively lethargy change and laboratory system and center of mass scattering angles. The elastic removal cross sections are

$$\Sigma_k^{g\to g+1} = \frac{q_k(u_g)}{\phi_k^g} \tag{3}$$

The group flux ϕ_k^g and the flux at the bottom of the group are determined from the weighting flux used. We then calculate the group scattering cross sections

$$\Sigma_{sk}^g = \frac{1}{\phi_k^g} \int_{u_{g-1}}^{g} du \phi_k(u) \sum_{k'} T_{kk'} \Sigma^c_{sk'}(u) \tag{4}$$

$$T_{kk'} = \frac{2k'+1}{2} \int_{-1}^{1} d\mu_c \, P_k[\mu_o(\mu_c)] \, P_{k'}(\mu_c) \tag{5}$$

[#]Based in part on the Master's Engineering Project of M. Danchak.

[*]Based in part on the Ph.D. Theses of G. Epstein, A. Ginsberg, S. Kang.

and then define the in-group cross sections by

$$\sum_k^{g\to g} = \sum_{sk}^{g} - \sum_k^{g\to g+1} \qquad (6)$$

Excellent results are obtained by this method as can be seen from Table 1. Running times, however, are dramatically improved, from 1790 to 290 cp seconds on the CDC 6600. Since about 90 cp seconds are associated with compilation, the improvement for this and similar problems from object programs would be a factor of about 8.5. (Degree of improvement for the code as a whole, of course, depends on the cost of non-elastic processing; e.g., resonance parameters and is therefore material dependent.)

At high energies, where anisotropy is most important, the principal concern with anisotropy is an "in-group" concern. Slowing down is influenced principally by inelastic scattering and by isotropic and linearly anisotropic scattering. Thus, one can make a reasonable estimate of the anisotropic removal cross sections and subtract them from the group anisotropic scattering cross sections to get accurate anisotropic in-group constants. Viewed in this light, the results of Table 1 are particularly meaningful.

The principal limitation of the new procedure is that removal to one group only is permitted. An extension to treat full elastic matrices has been formulated and effort is being initiated on implementation.

High-energy anisotropic analysis of spectra in depleted uranium with ENDF/B Versions I and II is essentially complete. A typical comparison with experiment is shown in Fig. 1. The calculation neglects the presence of ^{235}U in the depleted uranium. Inclusion of ^{235}U led to substantial errors at high energies due to the excessive ^{235}U fission caused by the large overprediction of the low energy flux. That overprediction with ENDF/B data previously was diagnosed[2] as due to large errors in low energy inelastic scattering data.

The curves in Fig. 1 are typical of those for the various radii and directions examined. The low energy zone has the overprediction of the flux already cited. In the high energy zone,

agreement is good except for the prediction of a dip in the flux in the low MeV range. The location of this dip corresponds to a peak in inelastic scattering effectiveness, as measured by the continuous slowing down ξ parameter.[2] These results confirm earlier speculation[2] (evaluation being difficult at that time because of lack of anisotropy in calculations and presence of ^{235}U fission) that the inelastic effectiveness in this peak region is too strong in both ENDF/B versions (I and II). The fact that results are similar in all directions indicates that angular distribution data are in reasonable condition.

Time-dependent spectrum calculations have been extended to 250 groups. (Many groups are desirable for following the slowing down process in heavy elements.) While, as expected, running time is quite short, some numerical difficulties have been encountered in evaluating the coefficients required for the analytic solution. Remedies have been proposed for these difficulties. Testing is in progress.

The program to calculate spectral transition in the vicinity of an interface using an escape probability method together with a separable slowing down kernel is now operating. However, numerical problems have been encountered in the solution. Current effort is directed toward modifying algorithms to deal with these problems.

The re-entrant hole code also is operating, but has yielded surprising results. Some errors in the program have been discovered upon checking the code. They are now being corrected.

REFERENCES:

1. H. Amster, in A. Radkowsky (ed.), Naval Reactors Physics Handbook, Vol. I., USAEC, 1964.
2. N. N. Kaushal, B. K. Malaviya, M. Becker, E. T. Burns and E. R. Gaerttner, "Measurement and Analysis of Fast Neutron Spectra in Depleted Uranium," Nucl. Sci. Eng., in press.

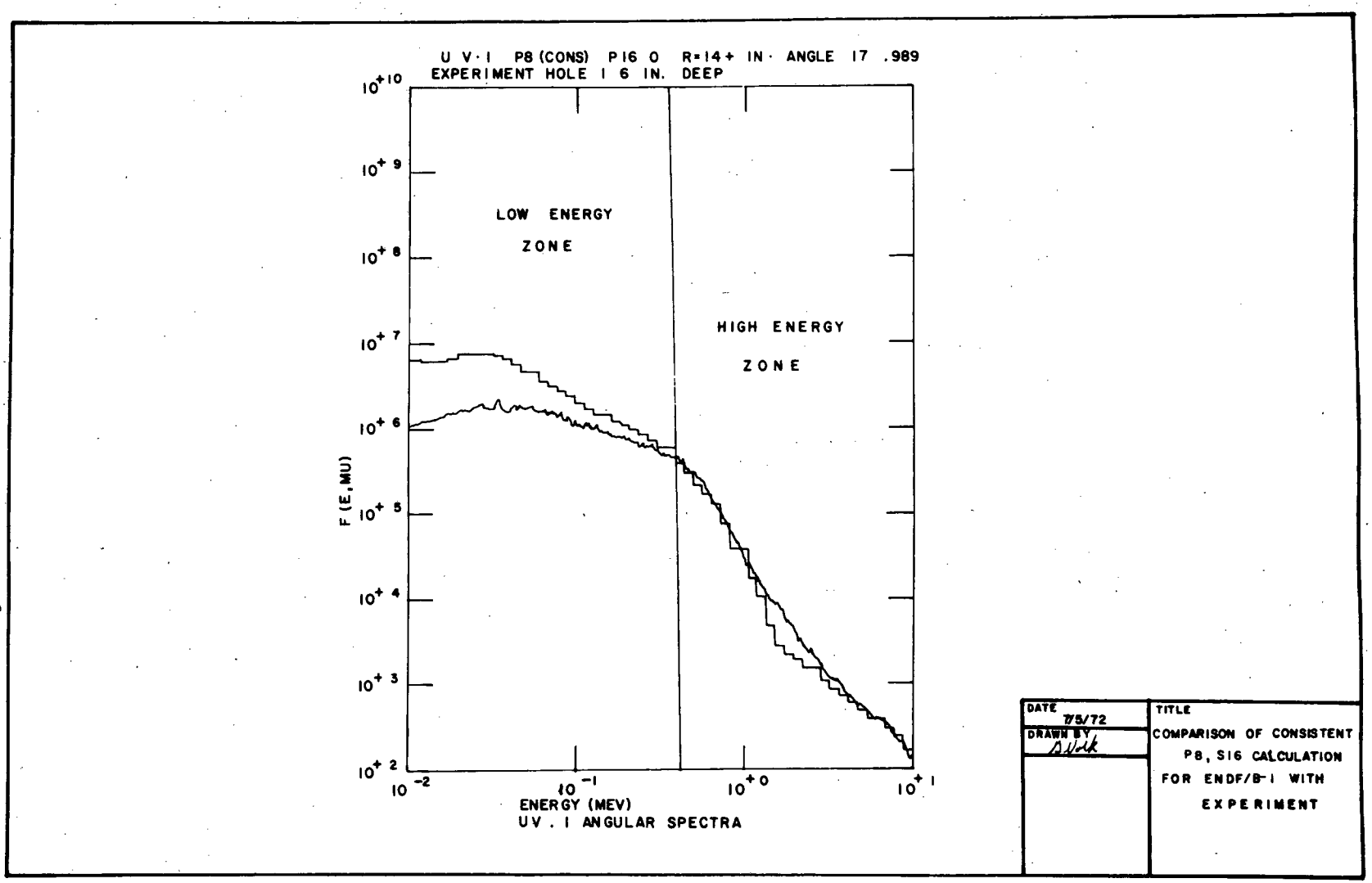
U V-1 P8 (CONS) P16 0 R=14+ IN. ANGLE 17 .989
EXPERIMENT HOLE 1 6 IN. DEEP
LOW ENERGY ZONE
HIGH ENERGY ZONE
F (E, MU)
ENERGY (MEV)
UV . 1 ANGULAR SPECTRA
DATE 7/5/72
DRAWN BY
TITLE
COMPARISON OF CONSISTENT P8, S16 CALCULATION FOR ENDF/B-1 WITH EXPERIMENT

Figure 1

Table 1

Comparison of New and Standard Group Constants from SUPERTOG for Elastic Scattering from Group 4 (5.35-6.87 MeV, Δu=.125) using ENDF/B-I Iron Data

	$\sigma_{4\to4}$			$\sigma_{4\to5}$	
Legendre Moment	New	Standard	Legendre Moment	New	Standard
0	2.37	2.37	0	.133	.132
1	1.81	1.81	1	.0253	.0248
2	1.34	1.34	2	.0131	.0133
3	.934	.938	3	.00901	.00856
4	.556	.557	4	-.00729	-.00684
5	.287	.288	5	-.00118	-.0110
6	.141	.141	6	-.00438	-.00468
7	.0673	.0692	7	-.000962	-.00115
8	.0275	.0296	8	-.00177	-.00159

COMPUTER DEVELOPMENT

INTERACTIVE GRAPHICS AT THE RENSSELAER LINAC

W. R. Moyer

Graphic representation of information is not new to science and technology. Point plots or curves representing data in two or more dimensions are a natural language of modern science. The chalkboard or pencil and paper are essential tools for investigators when discussing data. One wonders why interactive graphics is only now beginning to work its way into everyday use in the arts and sciences.

In the reactor physics field it is a case of "sink or swim." The sheer volume of data alone is enough to force an evaluation of data handling techniques, both in the generation of "raw" data from experiment and the subsequent processing and production of useful design parameters. A careful analysis of our particular data handling problems at the Rensselaer LINAC laboratory pointed the way to rapid visual and manual interaction between an investigator and his data.

Basic Philosophy

The ultimate goal of interactive graphic processing is to be able to provide the "lay" scientist (one who has neither the time nor the inclination to become an expert in computer languages) with visual control and command over steps in data processing and evaluation. Our approach to providing this facility is divided into two basic steps — the first of which has been initiated; the second step due to be taken about two years from now.

Step One - The first step consists of establishing a completely self-contained small computer with display hardware. To this end we have acquired a Digital Equipment Corporation Graphic-15 system. This system with the options as we specified provides a live visual display approximately 9" x 11" in size, a "light pen" for entering graphic information directly on the display screen, function push-buttons to call user subroutines and a keyboard for text or numerical entry of information. (See Appendix for a detailed list of hardware)

Although the system is small, and for this reason its performance will fall short of the ultimate goal, it will be of immediate use to the Rensselaer LINAC program.

Step Two - The second step consists of increasing the computing power and input/output capabilities of the Graphic-15 System by several orders of magnitude in order to meet the projected increased demands of interactive processing. This will be implemented by connecting the Graphic-15 system at Rensselaer by telephone to the AEC Computing Center at the Courant Institute in New York.

The technical approach will be to combine the transmission speed of remote batch operation with the real time capabilities of teletype terminal time-sharing. Figure 1 shows how such a system might be implemented using the Courant facilities. Presently a Honeywell DDP-516 computer handles the information flow between the CDC-6600 and its various remote users.[1,2]

The Courant CDC-6600 offers two types of service to the remote user. One is "batch" mode in which a "job" or deck of cards is entered as a unit into the job input queue. The deck is complete at input time with all commands, programs and data necessary to carry out the calculation. After the job is processed and the required output generated, the job is terminated. Rensselaer LINAC is currently using the remote batch facility with an IBM-1130 computer as a terminal.

Time-sharing is also available. A terminal for time-sharing is a low speed device such as a teletype which allows the operator to converse with a "real time" operating system. Programs are executed, parameters and data are entered, program flow changed — all at the operator's command from the terminal keyboard. Results are returned to the operator on the terminal typewriter for evaluation. To the time-share terminal operator, his program is on-line constantly interacting, accepting new values from the keyboard, producing requested output — remaining active until the operator commands job termination.

The proposed remote interactive graphics would be a unique combination of the speed of remote batch and the inter-

active capabilities of time-sharing. The Graphic-15 system will be connected to the time-sharing system to take advantage of the real time computation. Instead of an operator at a terminal keyboard, however, the Graphic-15 system under program control will handle all the conversational inquiries and responses necessary to operate the CDC-6600 time-share facility. The specific responses and commands given by the Graphic-15 system to the CDC-6600 will be generated in turn by interaction of a different nature between the Graphic-15 and its operator. Figure 2 is a block diagram showing this interaction.

Visual interaction, the natural language of the data evaluator, will be interpreted and converted by the Graphic-15 under program control to the conversational language required by the CDC-6600 time-share system. Results generated by the CDC-6600 will in turn be translated into appropriate graphic responses for the data evaluator. In short, the Graphic-15 system will be a two-way language translator enabling commands, program execution and parameter exchange between the data evaluator with his display screen and light pen and the CDC-6600.

To meet the speed requirements of remote interactive graphics, a 2000 baud dataset will be used, the same type as presently employed in the Rensselaer LINAC Remote Batch Terminal system. The higher speed dataset will allow a "conversation" between the CDC-6600 and the Graphic-15 at a nominal 16,000 characters per minute rather than the normal maximum teletype terminal speed of 10 characters per second.

This approach to remote interactive graphics; i.e., making an interactive graphic terminal look to the CDC-6600 like just an extremely fast typist, has the advantage that all existing CDC-6600 time-share software can be used without modification. Modification and development will be necessary, however, in the Courant DDP-516 software and hardware to allow the use of a high speed dataset in conversational mode. This sort of application of time-sharing is rather unique and would represent a significant

contribution to the art of remote processing. Discussions with Courant staff have indicated the technical feasibility of the approach described; adequate manpower at the Courant end might, however, be a problem in these times of shrinking funds.

Projected Use - Step One

In the experimental cross-section program, the "Step 1" graphics package will be immediately useful for such mundane, but nevertheless important, operations as determining backgrounds, delineating regions to integrate over resonance line shapes or to take resonance integrals, spectrum stripping, etc. "Raw" data from runs taken under different conditions can now be compared visually before being summed or discarded, eliminating the former tedious and time-plus-paper consuming task of listing and then comparing lists.

The graphics package will also be extremely useful in comparing our newer results with both ENDF evaluations and other experimental results; it is reasonable to expect that this system will lead to evaluation of specific cross sections at this laboratory. This system will be adequate for many analytical calculations in which accuracies of several percent are acceptable; e.g., R-matrix fits can readily be carried out for nuclides where a single channel dominates and the Doppler effect can be ignored; this would apply to mass ~50 nuclides where s-wave scattering dominates.

Within the framework of "Step 1", limited capability exists to perform theoretical calculations. In neutron cross-section theory, the calculational codes are generally too large for use on a PDP-15. The ability to run these codes on the CDC-6600 and have the output transferred via the IBM 1130 to the PDP-15 does exist for the present hardware. The PDP-15 can then display the CDC-6600 output for visual examination. For cross-section calculations which involve parametric studies and comparisons with reference data sets, the graphical display of output will serve to indicate behavior more clearly and point out side effects not normally detected. Other potential uses of the PDP-15 exist in the area of resonance parameter and cross-section manipulations obtained from our experiments. In the identification of cross-section coupling

schemes; i.e., single particle, two particle-one hole, one frequently needs properties of summed-weighted resonance parameter, such as strength functions and energy-averaged cross sections. Displays of such data as energy-averaged cross sections versus energy for different width energy-averaging intervals can both be calculated and displayed by the PDP-15, hence identifying the correct coupling schemes for more exotic calculations on the CDC-6600.

We have in the past made considerable use of the sensitivity of spectra to continuous slowing down theory parameters (age, resonance integral, slowing parameters) and of the sensitivity of these parameters to basic data. However, sensitivity analysis had to be done tediously by "brute force." Interactive graphics provides the potential for more extensive sensitivity analysis and therefore more detailed cross-section evaluation. We expect that continuous slowing down calculations, perhaps with some modification, are sufficiently simple that they can be performed on the PDP-15.

In the integral data testing program, the interactive graphics capability is expected to play a considerable role both in the processing of "raw data" and in the interpretation of the processed data in terms of assessment of basic cross sections. In the processing of raw data effects of uncertainties in the background, detector efficiency and other corrections necessary to arrive at the final spectrum, can be interactively assessed. The process of combining data from different detectors is better carried out and assessed on the interactive graphics. Large bulk storage capabilities of the PDP-15 make it easy to have quick recall of various spectrum data for comparison. This is particularly important for the integral measurements program where a large number of spectra must be measured and correlated. In the interpretation of processed data, the graphics will be useful in comparison of experimental results with theoretical calculations and in theory-experiment normalization. Adjustments of basic cross-section data or other parameters to obtain a good fit between experiment and calculation will be greatly facilitated by interactive graphics.

Particularly useful in this respect will be the capability to recall basic cross-section data to determine areas of uncertainty.

Projected Use - Step Two

Step Two gives us the ability to develop more sophisticated graphic programs for general use by our research group.

Automatic search routines are to be carried out to fit cross-section data which correct for multiple scattering, Doppler effects, resonance self-protection, etc. Stochastic calculations may be carried out in real (or almost real) time and compared with experimental averages. Eventually the graphics package will serve as the general Input/Output device for most of the more sophisticated data processing.

Having the joint capabilities of a CDC-6600 and PDP-15 Graphic system will add new dimensions to theoretical calculations. Within the neutron cross-section theory program, a strong dependence on parametric analysis is inevitable. Whether one is working with R-matrix theory, coupled-channeled or bound state calculational codes, a standard format is to vary certain input parameters representing physical entities in an attempt to fit experimental data or gain a grasp of parameter sensitivity in cross-section prediction. These computer calculations require the capability of a CDC-6600, but now we are in a position to monitor visually our parametric analysis via displays. For example in coupled-channeled calculations, displays of cross sections or strength functions versus imaginary potential strength along with their known experimental values would enable rapid decisions to be made on proper parameter variations, which would be forwarded to the CDC-6600 for further calculations. Also, many times the volume of cross-section output produced is so large that some interesting side effects may go unnoticed. By rapid graphical scanning of such output sets, these side effects can be efficiently detected and further analyzed. With the large storage facilities available on the CDC-6600, it now also becomes possible to display graphically several data sets or post calculational results simultaneously for relative comparisons.

As the on-line calculational capability increases, interpretation and analysis of fast neutron spectra will be further facilitated. Numerical and analytical spectrum calculations can be performed essentially on-line and compared with the experimental results. Sensitivity analyses can also be performed on-line. The greatly increased size of the data bank made available for quick reference should make evaluation of basic data files (in terms of our integral measurements) easier and more comprehensive. The net result is not only increased efficiency in the turnaround time between the time the experiment is performed and the time meaningful interpretation is obtained in terms of basic data, but also an increase in the breadth of analysis.

Performance to Date

The Graphic-15 system was installed at the Rensselaer LINAC and accepted in December of 1971. Already several user programs have been developed for local data reduction. The installation went smoothly and all benchmarks were satisfied easily. DOS-15, the the recently developed D.E.C. disk-oriented operating system is in use and running well.

REFERENCES:

1. R. P. Bianchini, "An Interface Between a Control Data 6000 Series Computer and a Honeywell 16-Bit Series Computer," Report NYO-1480-119, AEC Computing and Applied Mathematics Center, Courant Institute of Mathematical Sciences, New York University.
2. E. Franceschini, Y. Feinroth and M. Goldstein, "A Remote Entry System for the CDC-6600," Report NYO-1480-148, AEC Computing and Applied Mathematics Center, Courant Institute of Mathematical Sciences, New York University.

APPENDIX

Rensselaer LINAC Interactive Graphic System Equipment List

PDP-15 Computer - 16K words memory
KSR-35 Teletype
Disk memory - 262K word fast access
4 DECtapes
VT-15 Graphic Processor and Console
Light Pen
LK-35 Display Keyboard
6 Function Pushbuttons

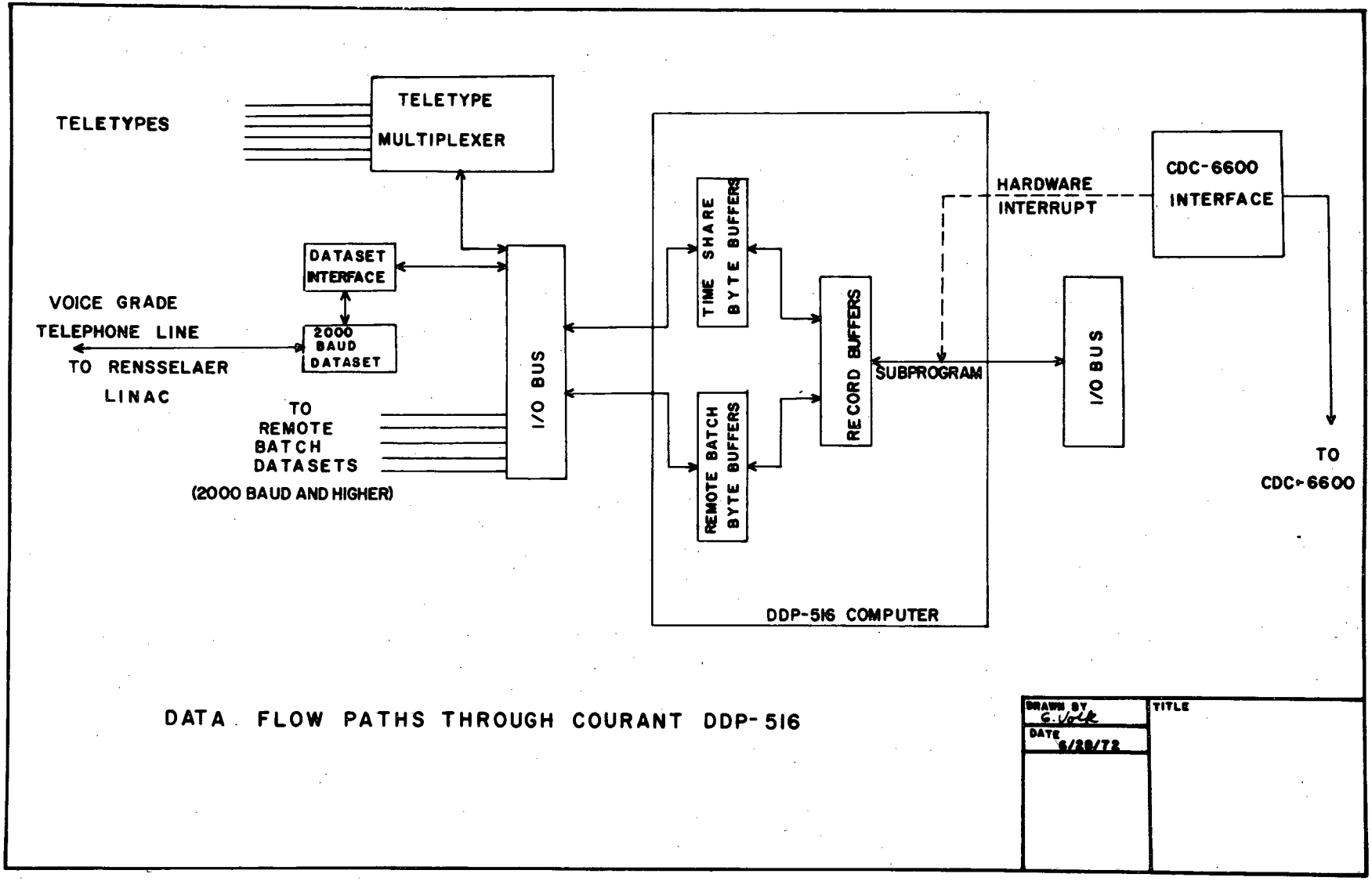
TELETYPES
TELETYPE MULTIPLEXER
DATASET INTERFACE
VOICE GRADE TELEPHONE LINE
TO RENSSELAER LINAC
2000 BAUD DATASET
TO REMOTE BATCH DATASETS
(2000 BAUD AND HIGHER)
I/O BUS
TIME SHARE BYTE BUFFERS
REMOTE BATCH BYTE BUFFERS
RECORD BUFFERS
SUBPROGRAM
I/O BUS
HARDWARE INTERRUPT
CDC-6600 INTERFACE
TO CDC-6600
DDP-516 COMPUTER
DATA FLOW PATHS THROUGH COURANT DDP-516
DRAWN BY G. Volk
DATE 6/28/72
TITLE

Figure 1

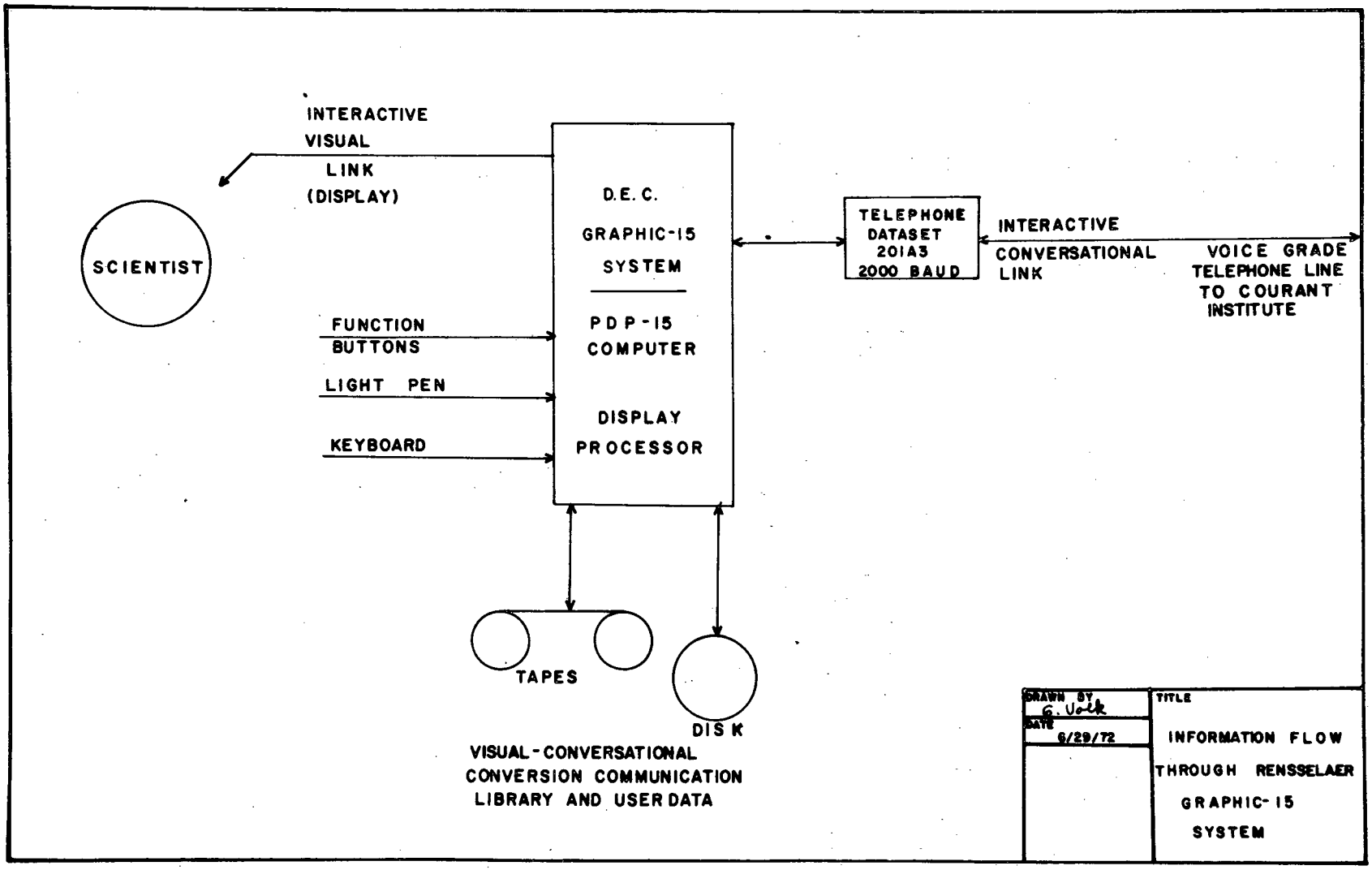
INTERACTIVE
VISUAL
LINK
(DISPLAY)
SCIENTIST
D.E.C.
GRAPHIC-15
SYSTEM
PDP-15
COMPUTER
DISPLAY
PROCESSOR
FUNCTION
BUTTONS
LIGHT PEN
KEYBOARD
TELEPHONE
DATASET
201A3
2000 BAUD
INTERACTIVE
CONVERSATIONAL
LINK
VOICE GRADE
TELEPHONE LINE
TO COURANT
INSTITUTE
TAPES
DISK
VISUAL-CONVERSATIONAL
CONVERSION COMMUNICATION
LIBRARY AND USER DATA
DRAWN BY
G. Volk
DATE
6/29/72
TITLE
INFORMATION FLOW
THROUGH RENSSELAER
GRAPHIC-15
SYSTEM

Figure 2